Politecnico di Torino

Politecnico di Torino

Master's degree Thesis in Automotive Engineering
A.Y. 2024/2025
Graduation session July 2025

Nonlinear contact model between wheel flange and tire sidewall

By
Mirzaakhmad Erkinov

Supervisors:
Prof. Carlo Rosso
Researcher Simone Venturini

Declaration

I hereby declare that the contents and organization of this dissertation constitute my own original work and does not compromise in any way the rights of third parties, including those relating to the security of personal data.

Mirzaakhmad Erkinov
2025

Nonlinear contact model between wheel flange and tire sidewall

Mirzaakhmad Erkinov

Politecnico di Torino, Department of Mechanical and Aerospace Engineering
Corso Duca degli Abruzzi, 24 – 10129 Torino, Italy

Contents

List of Figures

List of Tables

Abstract

This thesis presents the creation of an integrated finite element modelling approach for simulating the static and dynamic behaviours of automotive steel wheels under accelerated fatigue test loading conditions. The methodology is designed to enhance the design and validation process by reducing the dependence on experimental testing.

The main aspect of discussion is a method for managing interactions between tires and rims. The approach separates various loading factors, such as bead pre-tension, inflation pressure, and significant sidewall deformations occurring under high lateral load conditions. To improve computational efficiency in finite element analysis of automotive steel wheels under fatigue test loading, optimal linearization techniques are employed.

This thesis focuses on designing steel car wheels, with an emphasis on how various loads are transferred from the tire to the rim. Specifically, it examines the case of biaxial loading, which includes both radial and lateral forces. To investigate this, a finite element model with high complexity have been developed. The proposed method is analysed with ABAQUS CAE.

The accuracy of the model is assessed by comparing the simulated strain fields of the rim with experimental measurements. To facilitate this, an experimental setup was constructed to replicate the exact load conditions used in the simulations. Strains on the surface of the component were measured using strain gauges placed on both the spokes and the rim channel. These measurements were then compared with the simulation results at the same locations.

Finally, potential applications for the model are suggested. This makes the tool easy to incorporate into the development pipelines of industrial wheel.

Chapter 1: Introduction

1.1 Background Context

Automotive wheels significantly impact vehicle safety, handling, ride comfort, and fuel efficiency. A critical aspect of wheel performance involves the accurate modelling of interactions between the tire and the wheel rim. Despite advancements in material science and computational tools, accurately predicting the forces and stress distributions at the tire-rim interface remains complex due to the inherently nonlinear, multi-material nature of tires and their intricate geometry.

Traditional design methods heavily rely on physical prototype testing, which can be expensive, time-consuming, and limited by practical constraints. To address these limitations, the automotive industry increasingly employs advanced computational modelling methods to optimize wheel design while reducing reliance on physical testing.

1.2 Problem Statement

Automotive wheels have complex geometries and must meet multiple design criteria, including style, weight, manufacturability, and performance. While an aesthetic wheel design is important, it must also satisfy essential engineering requirements, such as durability and mechanical performance. Additionally, to ensure optimal driving performance and handling, the wheel must be as light as possible.

In the wheel industry, reducing wheel weight is a major concern since it not only improves vehicle efficiency but also lowers material costs for manufacturers. However, this weight reduction must not compromise the wheel's ability to withstand normal and extreme driving conditions.

Traditionally, wheel design and development has been a time-consuming process due to the need for extensive physical testing and multiple design iterations before mass production. In modern industry, reducing development time and minimizing the number of physical tests is crucial goal. To achieve these objectives, Computer-Aided Engineering (CAE) has become an essential tool in wheel design.

This study aims to develop and compare different FE model to improve the simulation of load transmission from the tire to the rim during the design process. Understanding this interaction is critical, as the resultant forces acting on the wheel are generally well known, but the way they are transmitted and distributed at the tire-rim interface remains complex. This is due to factors such as inflation pressure and the tire's intricate geometry.

The tire is a highly complex system, made of various materials with nonlinear behaviour, and it is connected to the rim through the beads. A deeper understanding of this interaction is essential for more accurate definition of contact behaviour between tire and rim and stress-strain analysis of the disc. This knowledge allows for an optimized wheel design that meets increasing demands for performance, lightweight construction, and reliability while also potentially reducing costs and development time.

While current computational approaches, such as Finite Element (FE) analysis, have provided significant insights into wheel performance, many existing models oversimplify the interaction between the tire and rim. In particular, simplified assumptions regarding frictional contact, nonlinear deformation of tire components, and dynamic load conditions limit the accuracy of these predictions. Consequently, current models often fail to capture critical interactions accurately, potentially leading to designs that are either overly conservative or insufficiently robust under real-world conditions. Therefore, there is a clear necessity for more sophisticated, validated computational models capable of realistically simulating tire-rim interactions under complex loading scenarios.

1.3 Objectives and Research Questions

The primary aim of this thesis is to develop, validate, and apply an advanced nonlinear finite element model capable of accurately simulating the interactions between automotive tires and steel wheel rims under realistic static and dynamic load conditions. Specifically, the thesis addresses the following objectives:

- *Objective 1:* Develop an integrated finite element model in ABAQUS capable of accurately capturing nonlinear contact behaviours between the tire and wheel rim, including frictional effects, bead-seat interference, and tire deformation.
- *Objective 2:* Validate the developed FE model through experimental measurements, employing strategically positioned strain gauges to capture accurate stress and strain distributions under controlled biaxial loading conditions.
- *Objective 3:* Investigate how different loading conditions, including radial, lateral, and combined load scenarios, influence the stress distribution and fatigue behaviour of automotive steel wheels.

To achieve these objectives, the thesis will address the following research questions:

- How do different load cases influence stress distributions at the tire-rim interface, particularly in critical regions such as the wheel flange?
- Can the developed FE model accurately replicate experimental results, providing confidence in its predictive capability for wheel design?
- Which modelling parameters (e.g., friction coefficients, material properties, and bead-seat interference conditions) most significantly affect the accuracy of FE simulations of tire-rim interactions?

1.4 Thesis Outline

The thesis is organized into five chapters as follows:

- *Chapter 2 – Literature Review:* Reviews existing methods and models used in simulating tire-rim interactions, highlighting strengths, limitations, and gaps that motivate the current research.
- *Chapter 3 – Methodology:* Provides detailed descriptions of the FE modeling approach, materials, contact definitions, experimental setups, and validation techniques.
- *Chapter 4 – Results and Discussion:* Presents comprehensive simulation results, detailed comparisons with experimental data, analysis of key stress distributions, and thorough discussion on the implications for wheel design.
- *Chapter 5 – Conclusion and Future Work:* Summarizes the main achievements, identifies current model limitations, and outlines specific recommendations for future research directions.

Chapter 2: Literature review

2.1 Introduction and Contextual Background

The interaction forces between the tire and the rim play a crucial role in wheel design, directly affecting structural performance, fatigue life, and overall vehicle dynamics. A precise understanding of these forces is essential for optimizing the design of lightweight and durable wheel rims. However, due to the complex structure of a pneumatic tire composed of multiple materials, reinforced layers, and exhibiting highly nonlinear behaviour accurately predicting the transmitted forces remains a significant challenge.

While extensive research has been conducted on the forces at the tire-road interface, far fewer studies have focused on the interaction between the tire and the rim. In many cases, the forces acting at the tire-rim interface are approximated using simplified load distributions, which, while convenient, may not fully capture the intricate force transmission mechanisms. This gap in the literature underscores the need for more refined modelling approaches to improve the accuracy of force estimation and enhance the efficiency of wheel rim design.

Several methodologies have been employed to analyse the behaviour of tires and their interaction with the rim. Finite Element (FE) models represent one of the most detailed and accurate approaches, offering high-fidelity simulations of tire deformation and force transmission. These models incorporate complex material properties and detailed structural configurations, allowing for precise force prediction. However, the high computational cost, extensive development time, and need for detailed tire construction data make FE simulations impractical for early-stage rim design and iterative optimization.

To address these limitations, simplified structural models have been developed to approximate tire behaviour using geometric parameters and inflation pressure. These models provide a reasonable estimation of the tire's load-bearing characteristics while significantly reducing computational requirements. Some studies have focused on modelling the radial stiffness of the tire, capturing its essential mechanical response without the complexity of full FE analysis. Such approaches are particularly useful in applications where rapid evaluation of tire-rim interaction forces is needed.

In addition to static load estimation, various analytical and semi-analytical models have been proposed to describe the in-plane dynamics of the tire. Rigid ring models, which treat the tire as a stiff circular structure, have been widely used to study vertical and longitudinal mechanical behaviour. While effective for basic load distribution analysis, these models often fail to capture the flexibility of the tire sidewalls and their contribution to force transmission. To overcome this limitation, flexible ring models have been introduced, allowing for the study of vehicle handling and low-frequency comfort by incorporating the elastic response of the tire sidewalls and inflation pressure effects.

Some of these analytical models have been extended to estimate tire-rim interaction forces more accurately. In particular, semi-analytical models that integrate structural deformation effects with simplified force transmission mechanisms have been proposed to bridge the gap between detailed FE simulations and purely empirical approximations. These models offer a balance between computational efficiency and accuracy, making them suitable for wheel rim design applications.

This chapter provides a comprehensive review of the existing literature on tire modelling approaches relevant to tire-rim interaction force estimation. It examines different modelling techniques, including FE simulations, analytical models, and experimental validation methods, highlighting their advantages and limitations. By analysing the state of the art, this review establishes the foundation for the semi-analytical approach proposed in this thesis, which aims to provide a computationally efficient yet accurate method for predicting tire-rim interaction forces.

2.2 Tire and Steel rims characteristics

The wheel's rigid structure is encased by a flexible component consisting of the tire and its inner tube, which helps maintain air pressure. In tubeless tires, the tube is not needed as the tire is sealed tightly to the wheel. Although this option is more expensive, it is preferred today for improved safety, as punctured tubeless tires lose air pressure more gradually.

A tire is a complex composite structure made of multiple layers of rubberized fabric, called plies, reinforced with cords. The orientation of these cords in relation to the tire's circumference gives each tire its specific mechanical properties. The angle between the cords and the tire's circumferential direction is known as the crown angle. Generally, lower crown angles improve vehicle handling, while higher angles, up to 90 degrees, enhance ride comfort.

2.2.1 Nomenclature of Tire and Steel Rims

Each tire is designated by a group of letters and numbers, as in the following example:

175/65 *R* 14 82 *T*

Where:

- The first figure (175) shows the dimension *W*, usually measured in mm; it is separated by a bar from the following figure. Because the tire is a deformable structure, this measure must be referred to an undeformed situation with correct inflation pressure and no load applied.
- The second figure (65) refers to the *aspect ratio* of the tire, given by the ratio *H/W* between the radial height and the width; aspect ratios are usually expressed as a percentage: In the given example *H* is 65% of *W*. If this figure is omitted it should be assumed to be 80%, long a standardized value.
- The following letter shows the type of tire plies; R stands for radial. The designation is otherwise omitted.
- The third figure shows the rim diameter in inches.
- The fourth figure is the *load factor,* which determines the allowed vertical load at an assigned inflation pressure; this figure is the row order of a standardization table where maximum allowed vertical loads are shown as a function of inflation pressure. This figure therefore has no physical meaning.
- The final letter indicates the maximum allowed speed for the tire.

Markings are assigned by the manufacturer. Steel wheels have embossed markings - each manufacturer places them differently, but it is usually found on the front of the wheel. Thanks to them, one can perfectly match the steel rim to the car. An exemplary rim designation may look like this:

17x7.5J 5x112 ET38 66.5

Where:

- 17 - rim diameter expressed in inches,
- 7.5 - rim width expressed in inches,
- J - is a flange profile dedicated to passenger cars,
- ET38 - is a car rim offset of 38 mm,
- 66.5 - diameter of the central hole expressed in mm.

Figure 1. Identification Markings on Steel Wheel Rims

2.2.2 Steel Wheel Rim Manufacturing Process

The most used car wheel is the disc wheel made of steel. Usually it is build up by two components, rim and disc. Today's steel wheels (rim and disc) are made of warm rolled steel with a high offset yield strength (>600 MPa). Both are sectionally weld together from the inside. Using a constant welding seam, would cause a massive distortion, that's why sectionally welding is the most proper method. The position of the welding seams needs always to be in the fewest dynamical driving load causing a minimum of alternating stress. Only this principle is assuring the fatigue resistance which as a vital characteristic over the live cycle of the wheels welding seams.

A coiler machine is an essential machine that is used before the rim welding. It provides the forms for coiled hoops from flat rim bands. It can be used in the preparation of wheels for light weight cars, trucks, construction vehicles, farm vehicles and more. After the feeding, deburring, stamping and auto coiling, the rim band will become a coiled hoop.

It is necessary to use the flattening machine to flatten the joint of the coiled rim bands that are over 4mm thick before proceeding to the flash butt welding process.

The welding slag will be produced on both the inside and outside surface of the weld joint after the welding process. A special machine unit comprised of the trimmer, planisher and end cutting machine can be used to remove the slag and make the surface of the weld joint flat and smooth.

After the weld joint processing, cooling, and re-rounding processes, a horizontal flaring machine will be used to flare two edges of the rim to make the following roll forming processes easier.

The roll forming machine is used for the symmetrical or asymmetrical roll forming of wheel rims for passenger cars, tractors and construction vehicles. This machine is used for the 1st through the 4th roll forming. The 4th roll forming process is optional and is used to press non-skid patterns onto the rim of tractors and construction vehicles.

A horizontal expanding machine is used for the expanding size process after the roll forming of the wheel rims. Precise expanding and sizing using a special tooling allows the formed rims to meet the design requirements for diameter.

Gas tightness detection tests are conducted to ensure the welding quality and reduce air leakage. The valve hole punching is done after profiling and is an important step in steel wheel rim manufacturing. With a corresponding Mold, it can punch the right valve hole on the effective part of the rim. The valve hole punching press is used for the flat pressing and hole punching on tubeless wheel rims.

A steel wheel is made of the wheel rim and the wheel disc. The wheel rim and tire form an airtight unit for bearing the vehicle’s weight and transmitting power. The wheel disc is connected to a hub and transmits the power from the engine. Usually, the wheel rim and disc of passenger cars and trucks are connected by welding, whereas large wheel rims and discs for farm vehicles are bolted to each other.

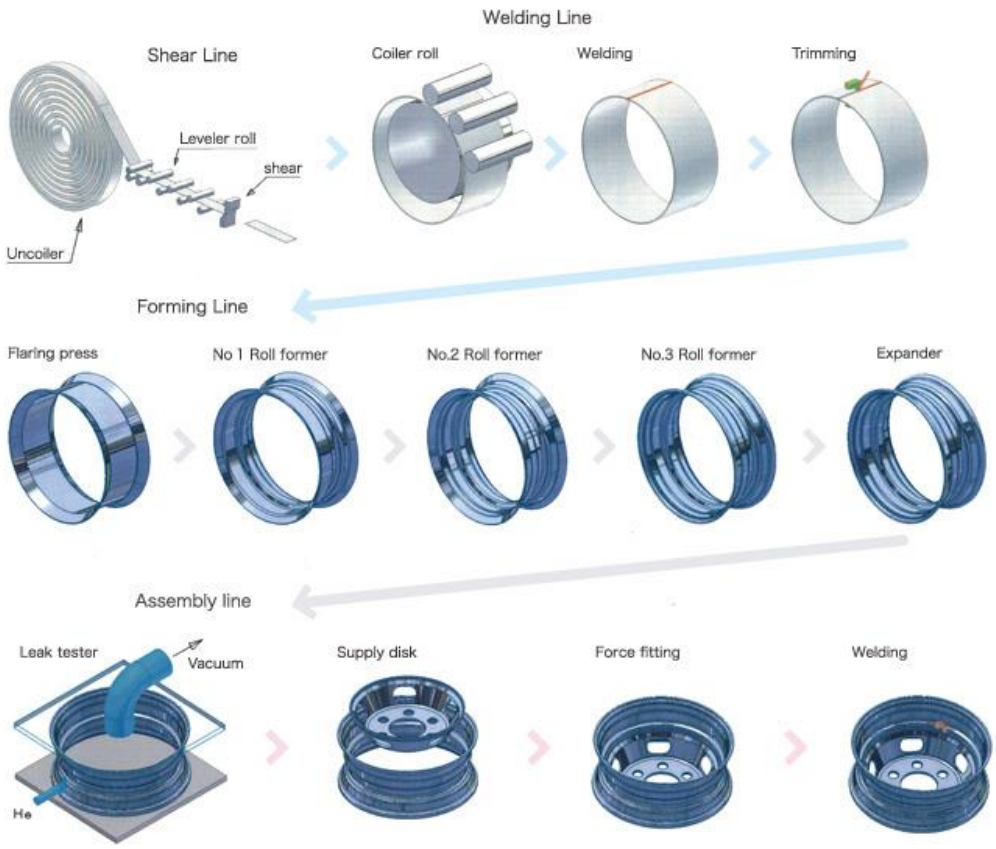

Figure 2. Automotive Wheel RIM Production Line.

2.3 Detailed Review of Tire-Rim Interaction Models

2.3.1 Finite Element (FE) Modeling

Finite element modeling represents one of the most advanced and detailed computational methods currently available for simulating tire-rim interactions. The FE method discretizes the tire and rim geometry into a finite number of elements, solving complex equations that describe structural deformation, stress-strain distributions, and contact conditions under realistic load scenarios. Software packages commonly used for these purposes include ABAQUS, ANSYS, and LS-DYNA.

Notably, FE models capture complex material behaviors of tires, such as nonlinear hyperelastic rubber characteristics, as well as frictional contacts between tire beads and rim seats, enabling high-fidelity stress analysis at critical interfaces.

Gobbi et al. (2016) presented a detailed FE model specifically focusing on the tire-rim interaction under motorcycle applications. Their work provided an accurate representation of the nonlinear deformation of tires, particularly highlighting bead-seat interactions under radial and lateral loading conditions. Similarly, comprehensive FE simulations have been conducted by Kim et al. (2008), who demonstrated the ability of detailed FE models to capture the nonlinear behavior and frictional contacts effectively. However, despite their high accuracy and predictive capabilities, these models are computationally intensive, often requiring significant computational resources and prolonged simulation times, thus limiting their feasibility for early-stage iterative design processes.

2.3.2 Analytical Modelling Approaches

Analytical models have traditionally served as valuable tools for rapidly approximating tire-rim interaction forces and behaviors. These methods use mathematical formulations based on simplified assumptions, describing tires as elastic structures with defined stiffness properties. Typically, analytical approaches involve simplifying the tire structure to curved beams or elastic shells, with linear springs approximating the interactions between the tire and rim.

For instance, early analytical models developed by researchers such as Pacejka (2002) provided fundamental mathematical formulations for tire behaviors based on empirical relationships. More specific to rim interactions, simplified analytical models have been proposed, representing tires as beams supported by radial springs to approximate the radial stiffness (Kim et al., 2008). Although these methods enable quick evaluations, their simplicity introduces substantial inaccuracies, especially under nonlinear deformation conditions and complex loading scenarios involving high lateral forces or frictional interactions. Consequently, their usage remains limited to preliminary design assessments and basic validation purposes.

2.3.3 Semi-Analytical (Hybrid) Models

Semi-analytical methods, also referred to as hybrid models, represent a bridge between purely analytical and fully numerical FE approaches. These methods typically combine analytical solutions of simplified tire-rim interactions with numerical methods to address nonlinearities and frictional behaviors more effectively. Such approaches aim to balance computational efficiency with moderate accuracy, allowing designers to evaluate numerous design iterations quickly yet reliably.

Gobbi et al. (2016) highlighted a semi-analytical approach combining beam theory for the tire's elastic structure with simplified finite element approximations of contact interactions. This methodology significantly reduced computational requirements compared to detailed FE models while maintaining moderate predictive accuracy. Similarly, hybrid models employing simplified ring or shell

models combined with analytical stiffness definitions have been explored by researchers aiming to strike a balance between accuracy and efficiency.

While semi-analytical models provide reasonable accuracy for intermediate design stages, they still lack the detailed fidelity necessary for accurate fatigue life predictions, especially in severe loading conditions and where frictional interactions significantly influence stress distributions.

2.3.4 Comparative Analysis of Existing Method

A comprehensive comparative summary of modelling approaches is provided below (Table 1), clearly outlining their descriptions, main advantages, and notable limitations:

Table 1. Comparative Summary of Tire-Rim Interaction Modelling Approaches

Methodology	Description	Advantages	Limitations
Finite Element	Detailed numerical discretization; nonlinear material and contact representation using software such as ABAQUS or ANSYS.	High predictive accuracy Detailed representation of nonlinear and frictional effects Robust under complex load conditions	Computationally demanding Requires detailed material and geometrical data Prolonged simulation times
Analytical	Simplified closed-form mathematical equations; tires modelled as elastic beams/springs.	Rapid computational speed Simple and quick preliminary evaluations Minimal data requirements	Significant oversimplifications Limited accuracy under complex load scenarios Ignores nonlinearities and frictional effects
Semi-Analytical	Hybrid approaches combining analytical beam or shell theory with simplified FE contact interactions.	Balanced computational efficiency and moderate accuracy Suitable for iterative design processes Enhanced accuracy over purely analytical methods	Reduced fidelity compared to full FE methods Limited accuracy for detailed fatigue predictions Less effective in severe nonlinear conditions

2.3.5 Identification of Research Gaps

Upon analysing the existing literature, several critical gaps emerge clearly, providing motivation and justification for further research:

- *Limited Nonlinear Frictional Interaction Modelling:* Existing analytical and semi-analytical methods typically inadequately represent nonlinear frictional behaviours and deformation at the bead-rim interface, significantly limiting the accuracy of predicted stress distributions.
- *High Computational Demand in FE Simulations:* While detailed FE methods offer accurate predictions, their high computational cost, simulation complexity, and need for detailed input data hinder their practical implementation for iterative and rapid design scenarios.
- *Scarcity of Comprehensive Experimental Validation:* Existing models often lack rigorous experimental validation, particularly under combined radial and lateral (biaxial) loading scenarios, leaving significant uncertainty about their real-world accuracy and reliability.

2.3.6 Motivation and Positioning of Current Research

Given the clear gaps identified thorough literature review, this thesis aims to develop an advanced and validated nonlinear FE model specifically addressing the shortcomings mentioned above. By explicitly incorporating realistic frictional conditions, nonlinear tire materials, and accurately capturing deformation under complex biaxial loading conditions, the proposed FE model represents a substantial advancement over existing modelling approaches.

Furthermore, an extensive experimental validation campaign is conducted, strategically employing strain gauge measurements to confirm and enhance the accuracy of the numerical predictions. The developed methodology thus contributes significantly to improving the reliability and efficiency of tire-rim interaction modelling, ultimately enabling more precise fatigue predictions, structural optimizations, and cost-effective automotive wheel designs

2.4 Tyre model

The model was initially developed in [21] to determine the distribution of pressure and shear stress/strain within the contact patch of a car tire subjected to a vertical load. In [25], the model was modified to calculate the tire-rim interface forces concerning the radial deflection of a tire.

The model is depicted in Fig. 4 and has been derived under the following hypothesis:

- The tread belt is described by a deformable curved elastic beam under small deformations with moment of inertia J and the material young modulus E.

- The tread belt is connected to the rim by means of a distributed linear spring k representing the residual radial stiffness per unit of length of the tire carcass.
- The rim is described by the internal rigid ring of Fig. 4 fixed to the ground.
- The tire is loaded in the radial direction and the model is symmetric with respect to a vertical axis passing through the centre of the tire.

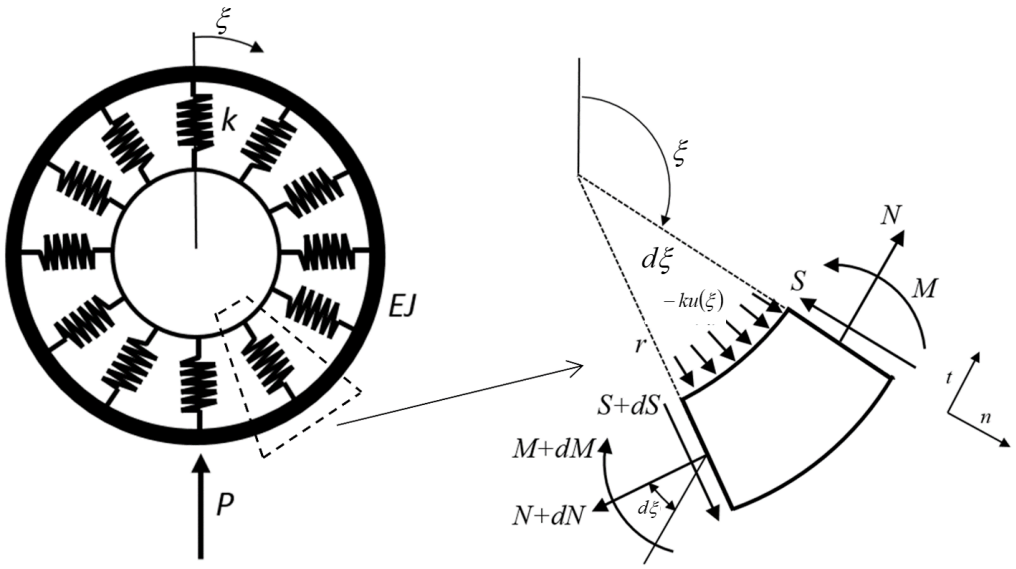

Figure 3. Simplified analytical tire model for radial direction. Left: tread belt modelled as a curved beam connected to the rim (fixed to the ground) by springs. Right: Free body diagram of a portion ds of the curved beam representing the tread belt.

The residual stiffness per unit length of the carcass, *k*, also accounts for the stiffening effect of the inflation pressure.

$$k = k_0 + k_1 \cdot P_i \tag{1}$$

where, according to the discussion of Section 2.1 and Section 2.2, the two coefficients of eq. 1 can be estimated as $k_0 = 2B_2$ and $k_1 = 2B_3$ (two sidewalls are considered).

Figure 5 illustrates the kinematics of a segment *ds* of the tread, defined by the infinitesimal angle dθ. By assuming a positive radial displacement *u* in the direction *n*, which shifts point *Q* to Q_d, and considering a radial vector *r* pointing toward the center, the following kinematic quantities can be determined under the condition $u \ll r$.

- Length ds_d of the deformed arch

$$ds_d = ds - \frac{u}{r} ds \tag{2}$$

- Angle $d\xi_d$ in the deformed configuration

$$d\xi_d = d\xi - \frac{d^2u}{du^2}ds \tag{3}$$

- Curvature in the undeformed configuration

$$\frac{1}{r} = -\frac{d\xi}{ds} \tag{4}$$

- Curvature in the deformed configuration

$$\frac{1}{r_d} = \frac{d\xi_d}{ds_d} \cong \frac{1}{r} + \frac{u}{r^2} + \frac{d^2u}{ds^2} \tag{5}$$

By analysing the kinematic quantities in Equations 2-5, the connection between curvature variation and the bending moment can be established

$$\frac{1}{r_d} - \frac{1}{r} = -\frac{M}{EJ} \tag{6}$$

In Figure 4 (Right), the forces acting on a segment *ds* of the curved beam are illustrated. By examining equilibrium in the radial and tangential directions, as well as rotational equilibrium, while disregarding higher-order terms, the following equations can be obtained

$$\frac{dS}{d\phi} = N = kru(\xi) \tag{7}$$

$$dN = -Sd\phi \tag{8}$$

$$S = \frac{1}{r}\frac{dM}{d\xi} \tag{9}$$

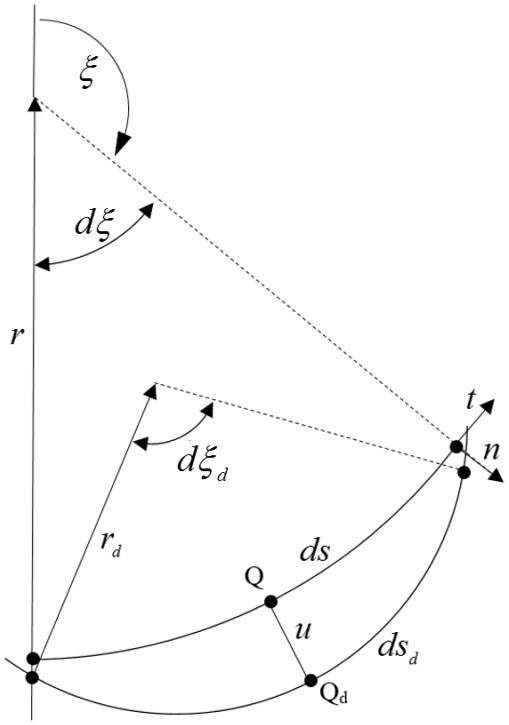

Figure 4. Portion ds of a general curved beam

Finally, by substituting Equation 9 into Equation 7, differentiating with respect to ξ, and considering Equations 8 and 6, the differential equation describing the relationship between the radial displacement $u(\xi)$ and the bending moment M is derived.

$$\frac{d^2u}{d\xi^5} + \frac{2d^3u}{d\xi^3} + \frac{\left(1 + \frac{kr^4}{EJ}\right)du}{d\xi} = 0 \tag{10}$$

Equation 10 is a homogeneous linear differential equation, whose general solution can be expressed as follows.

$$u(\xi) = U_1 e^{m_1\xi} + U_2 e^{m_2\xi} + U_3 e^{m_3\xi} + U_4 e^{m_4\xi} + U_5 e^{m_5\xi} \tag{11}$$

by defining $\delta = \sqrt{\frac{kr^4}{EJ} + 1}$, $\alpha = \sqrt{\frac{\delta-1}{2}}$ and $\beta = \sqrt{\frac{\delta+1}{2}}$, Equation 11 can be rewritten as

$$u(\xi) = C_0 + \cos(\beta\xi)\,[C_1 \cosh(\alpha\xi) + C_2 \sinh(\alpha\xi)] + \sin(\beta\xi)\,[C_3 \cosh(\alpha\xi) + C_4 \sinh(\alpha\xi)] \tag{12}$$

where the five constants can be computed by imposing the symmetry conditions $\frac{du}{d\xi} = 0$ both at $\xi = 0$ and $\xi = \pi$, the equilibrium of the shear force at $\xi = 0$ and $\xi = \pi$ and the conservation of the length of the beam. This last condition can be expressed as $\int_0^{\pi} \left(\frac{d^2u}{d\xi^2} + u\right) d\xi = 0$.

2.4.1 Forces acting on the rim

The focus shifts to the forces acting on the wheel rim. Only the reaction forces between the rim and tire in the radial and axial directions are considered, while circumferential forces resulting from the radial load are neglected, as they have minimal relevance in rim design. Figure 5 illustrates the forces acting at the tire-rim interface on an infinitesimal cross-section of the tire. The following sections provide an explanation of the forces in the radial and axial directions.

The forces per unit length in the radial direction consist of three contributing factors:

1. The force resulting from the inflating pressure is considered. The sidewall is modelled as a membrane element transmitting the tension force VV to the rim. The radial component of V is given by:

$$T_{rad,p} = Vcos(\phi) = \frac{ph_{f0}}{2\tan(\phi)} \tag{13}$$

   The radial component of the tension force in the sidewall, caused by the inflating pressure, is distributed between the rim and the tire bead. Specifically, a circumferential force arises on the bead, restricting its radial deformation. When the bead is stiff, the majority of the radial force due to pressure is transferred to the bead, with only a small portion acting on the rim. The exact distribution of this force depends on the specific tire. For the tire under consideration, the force is entirely exerted on the bead, meaning that the radial force on the rim is zero.

2. The radial reaction of the rim to the axial force is influenced by the axial component of V, which acts on the upper part of the rim, modelled as an inclined plane. This inclination can be approximated by identifying the region where the maximum pressure is applied. For the given rim, the inclination is approximately 25 degrees and is determined by the line connecting the endpoint of the fillet between the bottom and lateral contact zone of the tire to the separation point between the upper rim flange and the tire. Denoting the axial force acting on the rim as $\boldsymbol{T_{ax}}$ (calculated later), the corresponding radial projection due to the inclined plane can be determined as follows:

$$T_{rad,a} = T_{ax}\tan(\theta) \tag{14}$$

where θ represents the angle of action of the rim section in contact with the tire.

3. The extra force (relative to $T_{rad,p}$) resulting from the tire deformation under loading. The radial force per unit length, caused by the tire's deformation and acting on the wheel rim, can be calculated as

$$T_{rad,p} = \frac{\frac{1}{2} ku(\xi) 2\pi r}{2\pi r_{rim}} \tag{15}$$

where the scaling factor $\frac{2\pi r}{2\pi r_{rim}}$ accounts for the different values of the radius

of the tire and the rim and the coefficient 1/2 for the presence of two sidewalls.

The forces (per unit length) along the axial direction (i.e., the direction of the wheel's rotational axis) consist of two components.

1. Forces in the axial direction caused by pressure. Referring to the diagram in Fig. 6, and considering the deformation of the sidewall, the axial force can be written as

$$T_{ax,p} \cong \frac{ph(\xi)}{2} \tag{16}$$

2. Structural response of the sidewall. When the sidewall undergoes radial deformation, its curved shape causes it to also react in the axial direction. The magnitude of this axial force is influenced by the stiffness and geometry of the sidewall, as well as the stiffness of the connection between the sidewall and tread. The axial force can be calculated as

$$T_{ax,q} = \frac{k_{ax}}{k} T_{rad,q} \tag{17}$$

where k_{ax} is the axial stiffness of the sidewall. To estimate k_{ax}, different geometries have been evaluated by a FEM model and values of the axial stiffness between 20% and 40% of the radial one have been obtained. For the tire considered in this paper a value $k_{ax} = 0.3k$ is assumed.

The total forces applied to the rim are the sum of all the individual contributions and are expressed as

$$\begin{cases} T_{rad} = T_{rad,a} + T_{rad,q} \\ T_{ax} = T_{ax,p} + T_{ax,q} \end{cases} \tag{18}$$

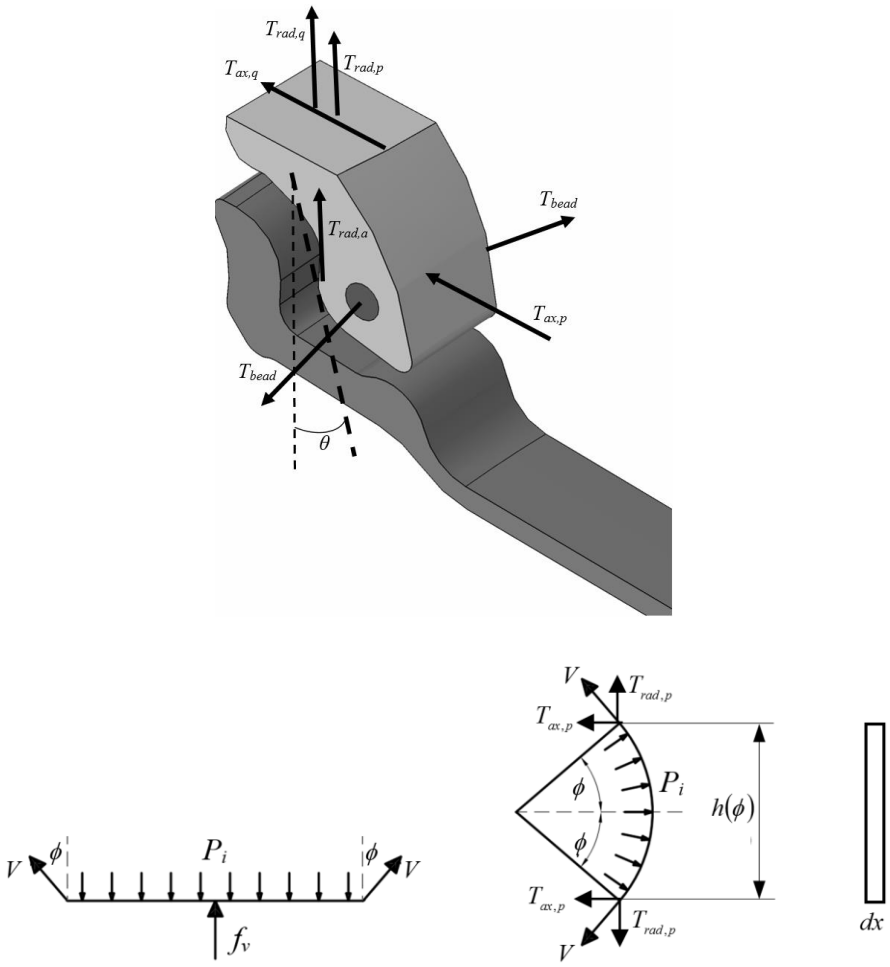

Figure 5. Forces acting at tire-rim interface on an infinitesimal section of the tire (up). Forces acting at tire-rim interface on an infinitesimal section of the tire (down).

Chapter 3: Methodology

3.1 Experimental campaign

This section presents the implementation of the stiff distributed interface. An experimental campaign is conducted using a biaxial test bench to measure strain variations at specific locations on the steel wheel geometry. The study includes an experimental-numerical comparison to validate the proposed methodology and highlight the limitations of a rigid interface in capturing nonlinear behaviour at the rim flange under high lateral load conditions.

Experimentally, stress histories are recorded using strain gauges placed on the steel wheel flanges. Additional strain gauges are positioned on the disc to facilitate result comparison. Numerically, stress histories are obtained from approximated averaged positions in the finite element (FE) model. The primary goal is to assess the effectiveness of the developed interface methodology in describing the stress distribution across the entire steel wheel geometry, with a particular focus on the rim flange region. To emphasize the flange behavior, a segment of a biaxial fatigue test campaign is analyzed.

As previously mentioned, flange behavior is significantly influenced by internal reactions between the tire bead and both the inner and outer flanges during operation. Generally, the inner and outer flanges exhibit different mechanical responses: the inner flange cross-section behaves like a cantilever beam, supporting higher stress on the channel, while the outer flange, due to its shorter arm-to-disc connection, provides a stiffer support. Flange deformations are measured during biaxial tests, with additional strain gauges placed primarily in the circumferential and axial directions on both inner and outer surfaces.

The experimental campaign is carried out using the ZWARP fatigue test, following the PV-5608 load test procedure. This procedure requires 117 repetitions of a set of 32 steps, where each step consists of 22 unique load cases with predefined radial and lateral loads. These loads are applied on the MTS test bench using the OMM procedure, as detailed in Table 2. Instead of performing the full fatigue test, a brief time history is recorded for each load case at a lower angular speed to facilitate comparison with numerical results. The MTS test bench is manually actuated, gradually increasing the loads and camber angle until the prescribed conditions are reached.

Table 2. ZWARP fatigue test load cases on 0215X with PV-5608 procedure.

Load case	F_z [N]	F_y [N]	γ [°]
1	16104	-5086	14.4
2	4238	-1695	6.7
3	10171	-1695	5.2
4	5792	-1413	5.2
5	16104	0	0.0
6	7628	0	0.0
7	6357	283	0.0

8	10171	1695	-5.3
9	6498	1695	-7.6
10	7063	2825	-10.2
11	8970	4238	-13.6
12	12361	4309	-12.6
13	16104	5086	-14.4
14	10171	5227	-14.3
15	8829	5651	-14.3
16	10736	7063	-15.0
17	15257	7134	-15.0
18	13279	7134	-15.0
19	12714	8476	-15.0
20	14126	8970	-15.0
21	16881	9041	-15.0
22	20623	10311	-13.0

Given that the study focuses on stress behaviour in the steel wheel flanges, testing is performed on the 0215X steel wheel model—a recently reworked design based on a wheel that previously experienced high-cycle fatigue failure at the outer flange. Table 3 provides the specifications of the steel wheel and its associated tire.

Table 3. 0215X steel wheel and tyre specifications.

Characteristic	**Property**	**Value**
Tyre	Model [-]	215/55 R16
	$P_{rel,}$ relative inflation pressure, [Pa]	4.5e5
Wheel	Model [-]	215x16H2
	EH, offset [mm]	49
	N_b, number of bolt holes [-]	5
	T_n, tightening torque [Nm]	120
Disc material	grade material [-]	MW06
	t, thickness [mm]	4.2
Flange material	grade material [-]	MW05
	t, thickness [mm]	1.55÷2.4

3.1.1 Strain gauge positioning

The thesis presents a methodology for strain gauge positioning on steel wheels to enhance the accuracy of stress measurements under operational loading conditions. The positioning approach is based on a strain-geometrical selection criterion that identifies optimal locations for strain gauge placement by maximizing strain sensitivity while minimizing computational effort. This method ensures that the most critical regions of the structure, where strain variations are significant, are effectively monitored. Inspired by the Modal-Geometrical Selection Criterion (MoGeSeC) [21], initially developed for sensor placement in structural dynamics, the approach selects master nodes by evaluating the strain distribution and geometrical properties of the wheel under different loading conditions.

To achieve reliable strain measurements, a total of twelve KYOWA KF-GS-1-350-C1-11 strain gauges were strategically placed on the inner and outer flanges of the wheel in the experimental test. These positions were determined through finite element simulations using ABAQUS®, which provided insight into the stress components acting on the wheel, particularly the circumferential and radial/axial stresses. The finite element model incorporated realistic loading scenarios to replicate operational conditions, allowing for a refined selection of strain gauge locations. The primary goal was to ensure that the gauges captured the most critical stress variations experienced by the wheel during fatigue testing.

Experimental validation confirmed the effectiveness of the proposed strain gauge positioning strategy. The study identified six key locations for strain gauges, detailed in Table 4 of the thesis, which provided optimal coverage of the stress distribution on the wheel's surface. The selected gauges on the inner flange (R1–R4) were mainly oriented to measure radial stresses, while those on the outer flange (R3, R6) were positioned to capture circumferential stresses. The placement strategy accounted for the uncertainties associated with experimental testing, such as sensor alignment and mounting imperfections, which were addressed by refining the numerical model and cross validating the results with real-world fatigue tests.
The research also explored the influence of different adhesives and coatings used to secure the strain gauges, ensuring durability and accuracy in long-term testing conditions. Additionally, a systematic comparison between numerical and experimental results helped to calibrate the finite element model, improving its predictive capability for stress analysis in steel wheels. The optimized strain gauge positioning methodology contributes to more accurate fatigue assessments, reducing the need for extensive experimental trials while improving the reliability of structural evaluations. This study offers a valuable framework for strain measurement in automotive wheel testing, supporting future advancements in wheel design and durability assessment.

Table 4. 0215X experimental strain gauge positions.

Channel	X[mm]	Y[mm]	Z[mm]	ρ [mm]	θ [°]	Surf. [-]	Dir[-]
R1	0	-74.8	-215.6	215.6	0	Inner	Radial
R2	187.3	-81	108.2	216.3	240	Inner	Circ.
R3	-203.9	-88.5	117.8	235.5	120	Outer	Circ.
R4	0	74.8	-215.6	215.6	180	Inner	Radial
R5	187.5	81	108.3	216.5	60	Inner	Circ.
R6	-203.9	88.5	117.8	235.5	-60	Outer	Circ.
D1	0	-94.5	140.5	140.5	90	Outer	Circ.
D2	0	-81.8	117	117	90	Inner	Radial
D3	0	-90.5	151	151	90	Outer	Circ.
D4	23.8	-73.8	178.4	180	86.2	Inner	Tan.Edge
D5	0	-57	76	76	90	Outer	Radial
D6	45	-53.2	53.6	70	70	Outer	Radial

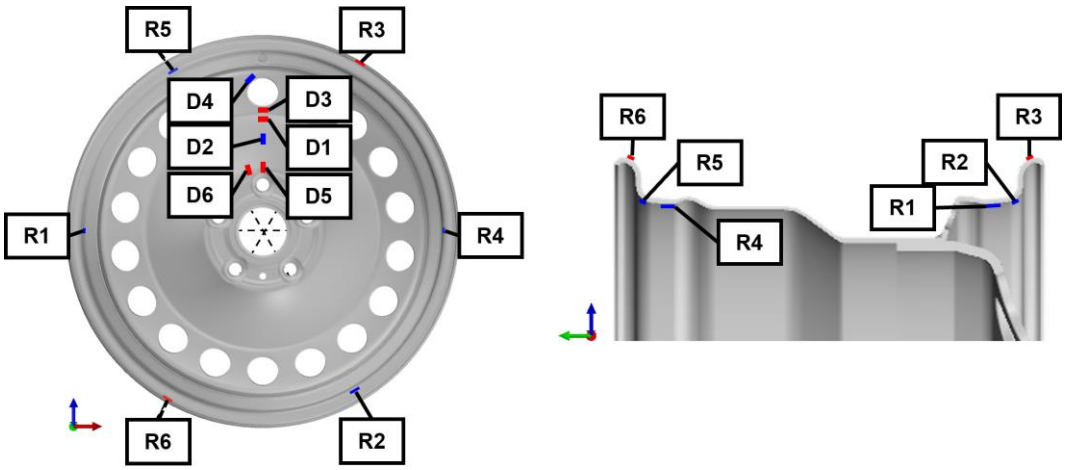

Figure 6. Position of strain gauges: orientation on XZ plane (left) and on cross-section (right).

3.2 FE models of the Rim and Tire

The goal of this sub-section is to create an ABAQUS finite element (FE) model that closely replicates a real wheel under radial and lateral loads in service conditions. It's necessary to investigate all the parameters required to describe each material type and every contact between parts. This can be a significant limitation for the model, as such information is often difficult to obtain or unavailable. Additionally, this model has the longest computational time compared to others developed, due to the large number of nodes and the highly non-linear materials involved. As a result, a very powerful computer is required to run the simulation.

3.2.1 The Rim

The 3D model of the Rim has been provided by the supplier and pre-processed in CATIA V5 software and imported in ABAQUS as STEP FILE. Its geometry and dimensions is similar to typical steel rim that is used in the real-world applications. Figure 7 illustrates the front and isometric view of the rim with it tangent curvatures.

Figure 7. 0215X Automotive steel rim. Front and Isometric views.

The material chosen for our analysis is HSLA steel which is typical composition for automotive wheels. Also Aluminium, Magnesium, Silicon-Copper and Titanium alloys are widely used in the automotive industry. In general the deformation of the steel wheel is negligible, but to replicate the real world conditions, the residual stresses, due to the interference fit of the disk into flange, is considered. That is why it is necessary to define the HSLA material with its stress-strain data along with Elastic modulus($\boldsymbol{E}$) and Poisson ratio($\boldsymbol{\upsilon}$):

Table 5. Material properties of steel rim.

Material	Property	Value
HSLA steel	ρ, density [kg/m^3]	7850
	E, Young modulus [GPa]	203
	ν, Poisson ratio [-]	0.3

Due to the detailed nature of this part, which includes sharp fillets and complex geometry, it is more convenient to define mid-plane of the geometry of the rim and define the part as a shell element (type S4). This technique will reduce the cost of the analysis significantly.

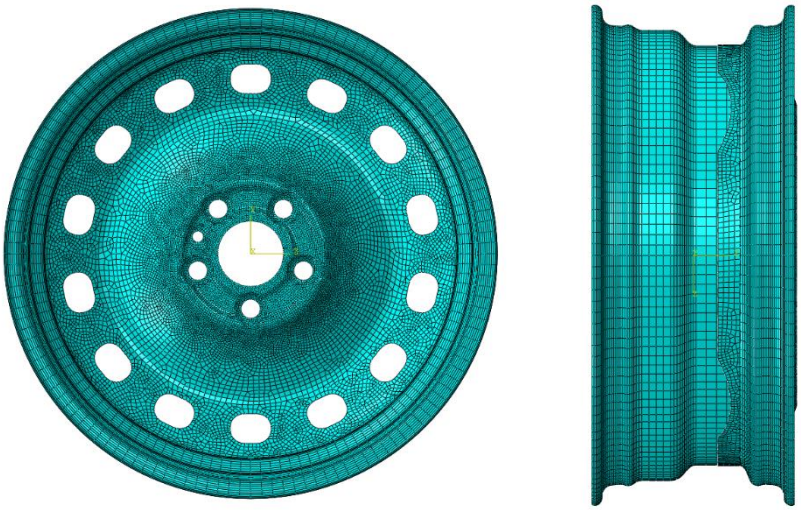

Figure 8. Mesh of the rim.

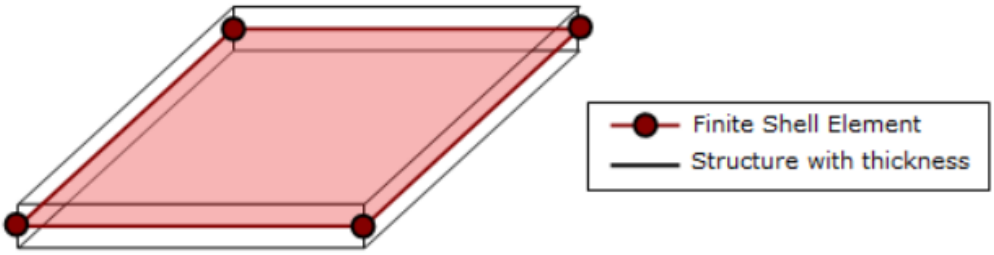

Figure 9. S4 shell element type used to mesh the rim.

3.2.2 The Tire

The section of the tire is obtained from real 215/55 R16 tire and then simplified to reduce the complexity of the geometry shown in the Figure 10. The section then was sweep extruded using CATIA V5 along the circle path to obtain the model. As it is visible from the figure, 3D model of the tire has been partitioned into several cell for two reasons:

- Partitioning of the complex geometries helps to have more regular hexagonal mesh along the curved profiles.
- Different material properties can be assigned to the partitioned cells.

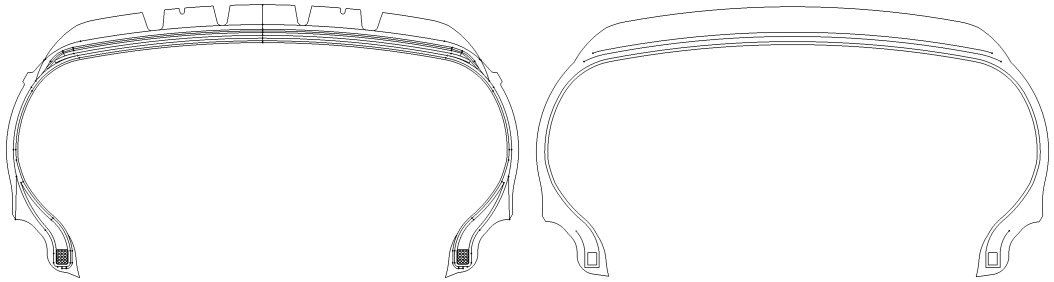

Figure 10. Real tire section left, Simplified tire section right.

The tire is a complex body because it consists of different layers and different materials with its own properties. But for the sake of simplicity and minimum requirements for the accuracy of the tire analysis, we consider only main components like tread, undertread, sidewall, plies, carcass and bead. To replicate it in our analysis in the most possible, the FE model layers are be obtained by partitioning the body into different cells like shown in the Figure 11. The bead is a conventional steel. The property definition of rubber parts (tread, undertread and sidewall) a Mooney-Rivlin model has been implemented. Tire nylon reinforcements of carcass and plies have been implemented by means of composite layers with their own orientation with the respect to circumferential direction of the tire, for carcass 90° and for plies ±20°. The geometric and material reference values were taken from literature.

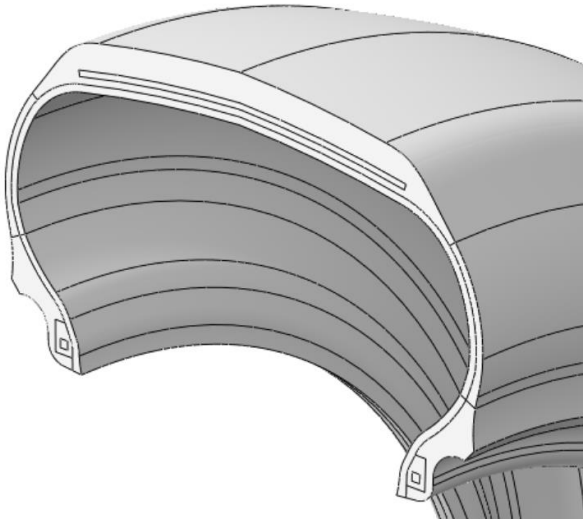

Figure 11. Cross-section of the tire CAD model.

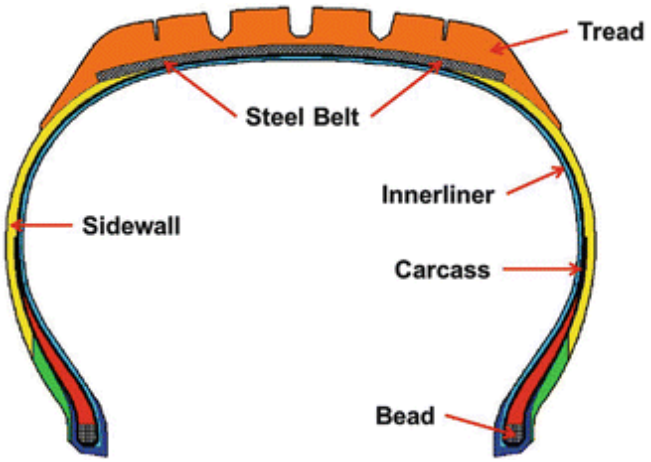

Figure 12. Tire composition.

Table 6. Tire composition and properties.

MATERIAL	**Material type**	**Property**
Tread	*Mooney-Rivlin (rubber)*	C_{10}=0.8061, C_{01}=1.805, D_1=0, ρ=1.125e-3 g/mm^3
Undertread	*Mooney-Rivlin (rubber)*	C_{10}=0.1401, C_{01}=0.427, D_1=0, ρ=1.125e-3 g/mm^3
Bead Filler	*Mooney-Rivlin (rubber)*	C_{10}=14.14, C_{01}=21.26, D_1=0, ρ=1.125e-3 g/mm^3
Sidewall	*Mooney-Rivlin (rubber)*	C_{10}=0.1718 C_{01}=0.8303, D_1=0, ρ=1.125e-3 g/mm^3
Carcass	*Isotropic (textile fabrics)*	E=3970 *MPa*, ν=0.45
Plies ±20°	*Isotropic (steel)*	E=210 *GPa*, ν=0.3 ρ=7.85e-3 g/mm^3
Bead	*Isotropic (steel)*	E=210 *GPa*, ν=0.3 ρ=7.85e-3 g/mm^3

This part is measured using linear hexahedron element (type **C3D8H**) following a sweep mashing technique (Figure 14). C3D8H is an eight-node hexahedral hybrid finite element used in finite element analysis (FEA), particularly in Abaqus software. The element is a brick with eight corner nodes. It is useful for modelling incompressible or nearly incompressible materials such as rubber, soft tissues, and highly plastic metals. It has a first order (linear) interpolation function for displacement fields. The additional degree of freedom ensures numerical stability in incompressible materials. The advantages are that it prevents volumetric locking, which occurs in standard elements when modelling nearly incompressible materials and it is computationally efficient compared to higher-order elements like C3D20H. On the other hand, C3D8H has some disadvantages that it is lower accuracy for bending-dominated problems compared to higher-order elements and it is more computationally expensive than standard C3D8 due to the additional pressure degree of freedom.

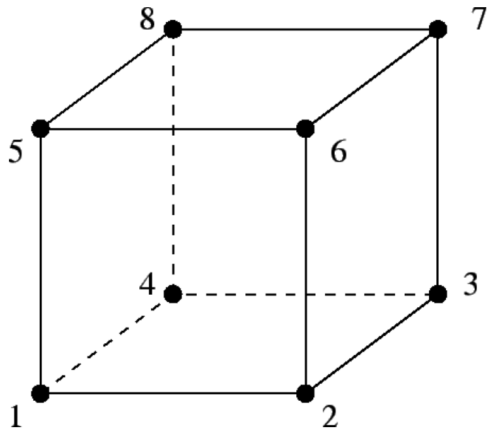

Figure 13. C3D8H hexahedron element type.

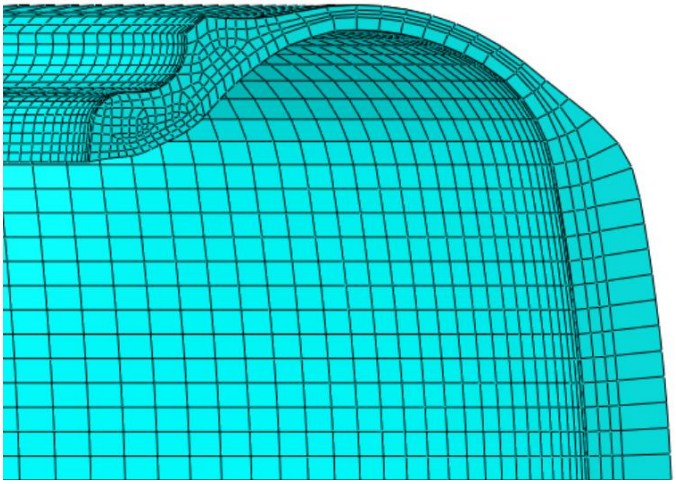

Figure 14. Half section of the meshed tire.

3.2.3 Assembly, Interactions and Constraints

The rim and tire are assembled and aligned coaxially to ensure proper interaction between the components. To accurately simulate the mechanical behaviour of the system under various loading conditions, a 3D rigid planar surface is introduced. This surface represents a highly stiff rough steel plate, significantly more rigid than the tire, which serves to transmit different applied loads effectively. The rigid surface is carefully positioned within the assembly, placed perpendicular to the symmetry plane of the system. It is also located sufficiently far from the wheel's centre which coincides with the origin of the global coordinate system to prevent any unintended interaction with other parts during the initial phase of the simulation. This strategic placement ensures that the influence of the steel plate on the overall structural response is accurately captured.

To facilitate a precise and efficient numerical analysis, the rigid planar surface is meshed using large linear quadrilateral elements (type R3D4). A structured meshing technique is employed to enhance the quality of the finite element model, ensuring accurate force distribution and improved computational stability. The structured mesh helps maintain uniform element sizes and shapes, reducing numerical errors and improving convergence during the simulation process.

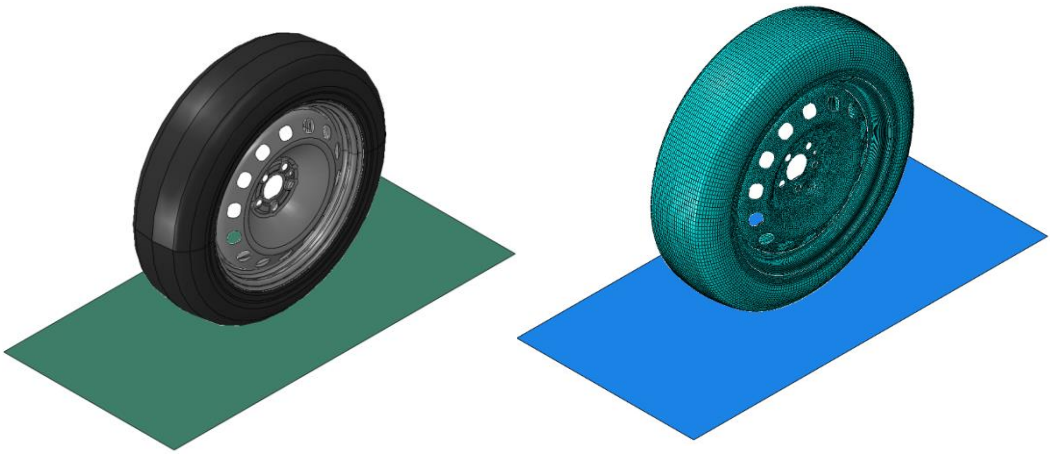

Figure 15. Assembly of the tire and rim. Assembly default right and Mesh default left.

Table 7. Summary of Finite Element Mesh Statistics for the Whole Assembly, Tire, and Rim

Characteristic	Property	Value
Whole assembly	# Nodes	156038
	# Elements (S4, S3, C3D8H)	133943
Tire	# Nodes	128705
	# Elements (C3D8H)	107184
Rim	# Nodes	27333
	# Elements (S4, S3)	26759

All interactions between surfaces are carefully defined to prevent material interpenetration and to accurately simulate friction in the designated contact areas. This ensures a realistic representation of the physical behaviour of the components under different loading conditions. The contact definitions help maintain proper force transmission, allowing for accurate simulation of mechanical responses such as load distribution, deformation, and slip at the interfaces:

- *Frictionless Contact Between the Bead and Bead Seat*. In the simulation model, a frictionless contact condition is defined between the tire bead and the bead seat of the rim. This setup ensures that the tire and rim do not interpenetrate in the radial direction while still allowing relative movement between the two components. The absence of friction in this region facilitates slip during the inflation phase, enabling a more realistic representation of how the tire seats itself onto the rim under internal pressure.
  Although friction is naturally present at the bead seat in real-world conditions and contributes to force transmission, it is intentionally omitted in this model to simplify the contact behaviour. Instead, frictional effects

are only considered at the rim flange, where they play a critical role in preventing axial displacement. This modelling choice is justified because the axial forces generated by air pressure are ultimately constrained by the contact at the flange. Consequently, neglecting friction at the bead seat does not significantly impact the overall force balance or structural response of the tire-rim system.
To accurately replicate the physical interaction between the components, a surface-to-surface contact approach is employed. This method ensures that normal contact forces prevent penetration while allowing the necessary sliding motion. A zero-friction coefficient is assigned to the bead seat interface, maintaining unrestricted movement during inflation and ensuring that the simulation captures the natural seating process of the tire without introducing artificial constraints.
Furthermore, this contact definition contributes to a more stable numerical analysis by reducing excessive constraints that could otherwise lead to convergence issues. By localizing frictional effects to the rim flange and employing a structured contact strategy, the model achieves a balance between computational efficiency and mechanical accuracy, making it well-suited for analysing tire-rim interaction forces under realistic loading conditions.

- *Contact with Friction Between the Sidewall and Rim Flange*. A contact condition with friction is defined between the tire sidewall and the rim flange to prevent the beads from moving beyond the flange, ensuring that the air pressure remains contained within the tire. This contact plays a crucial role in maintaining the stability of the tire-rim assembly, especially under varying loading conditions.
  To accurately capture the interaction, a surface-to-surface contact model is used, incorporating both normal and tangential behaviour. The normal contact prevents interpenetration, while the tangential behaviour accounts for frictional resistance. A friction coefficient of $\mu = 0.75$ is assigned to this interface, which is sufficient to prevent unwanted slippage and maintain proper seating of the tire on the rim.
  This frictional constraint not only contributes to the mechanical integrity of the assembly but also helps distribute forces effectively, especially when external loads, such as cornering or braking forces, are applied. By incorporating realistic contact properties, the simulation provides a more accurate representation of the tire's response to operational conditions.

- *Contact with Friction Between the Rigid Plate and the Tire* (Fig. 17). A frictional contact condition is defined between the rigid plate and the tire to prevent interpenetration and ensure proper load transmission. This contact setup is essential for accurately simulating the interaction between the tire and a rough surface, reflecting real-world conditions where the tire contacts the ground or other rigid elements.
  A surface-to-surface contact model is implemented, incorporating both normal and tangential behaviour. The normal behaviour prevents the rigid plate from penetrating the tire, ensuring realistic force distribution, while the tangential behaviour introduces frictional resistance to simulate realistic traction effects.

A friction coefficient of $\mu = 0.8$ is assigned to this contact interface, which closely replicates the interaction between a tire and a rough surface, such as asphalt. This high friction coefficient ensures that the tire experiences appropriate grip and force transmission, preventing excessive slip and enhancing the accuracy of the simulation when modelling braking, acceleration, or lateral forces.
By defining this contact condition with appropriate friction properties, the model can more accurately represent real-world tire behaviour, particularly in scenarios where tire-road interaction plays a critical role in performance and safety assessments.

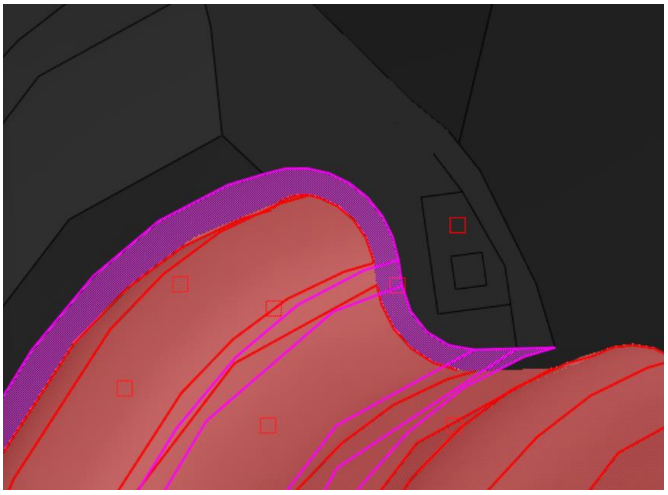

Figure 16. Representation of the contact between tire and flange.

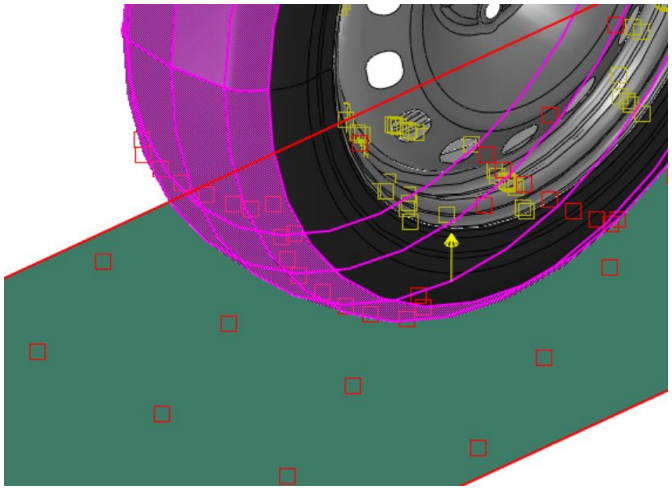

Figure 17. Representation of the contact between tire and ground.

3.2.4 Procedure Steps and Boundary conditions

The primary finite element model is developed within the ABAQUS® environment, ensuring a robust and accurate simulation of the tire-rim interaction. The model's structure and the computational procedure steps are systematically outlined in Figure, providing a clear overview of the key steps involved in the analysis.

To ensure accurate and reliable simulation results, it is essential to account for residual stresses introduced during the production process. These stresses can significantly influence the structural behaviour of the wheel assembly, affecting both its strength and performance under operational loads.

To address this, a dedicated section in the simulation focuses on the introduction of residual stresses by replicating key aspects of the manufacturing process. At the current stage, the simulation incorporates press-fit assembly of the disc and rim as well as bolt tightening procedures, both of which contribute to the overall stress state of the system.

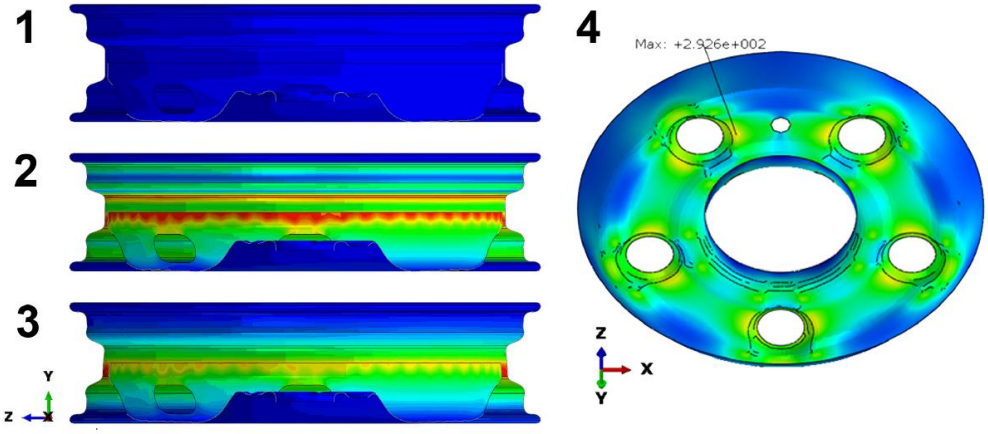

Figure 18. Residual stress preliminary simulation steps: 1) locking, 2) Figure. Residual stress preliminary simulation steps: 1) locking, 2) interference, 3) springback and 4) bolt tightening. (von Mises stress).

The analysis is conducted under a static regime, as dynamic effects are assumed to be negligible. This simplification is justified by the CDTire/3D model, which treats the rim as an infinitely rigid body, meaning that its dynamic behaviour has only a marginal impact on the simulated operating conditions. By adopting this approach, the computational complexity is reduced while maintaining a high level of accuracy in representing the tire-rim interaction forces. Therefore, the simulation is divided in different steps:

- *Structural locking*: Constraints are applied to the rim flanges and disc hub. Since the mesh represents the nominal dimensions of the components, overclosure takes place.

- *Interference*: ABAQUS® resolves the initial overclosure by adjusting the positions of the rim and disc nodes. This process introduces residual stresses

not only in the interference region but also throughout the geometry due to the applied constraints.

- *Springback*: The constraints on the disc hub and rim flanges are lifted and replaced with a constraint for axle hub rotation and a disc contact constraint.
- *Bolt tightening*: Equivalent concentrated nodal forces are applied to the regions around the bolt holes.
- *Tire mount*: The pre-simulation CDTire load profile is applied as concentrated nodal forces to the rim flange regions.
- *Loading*: The hub of the rim is loaded according to the experimental test loading scenario.

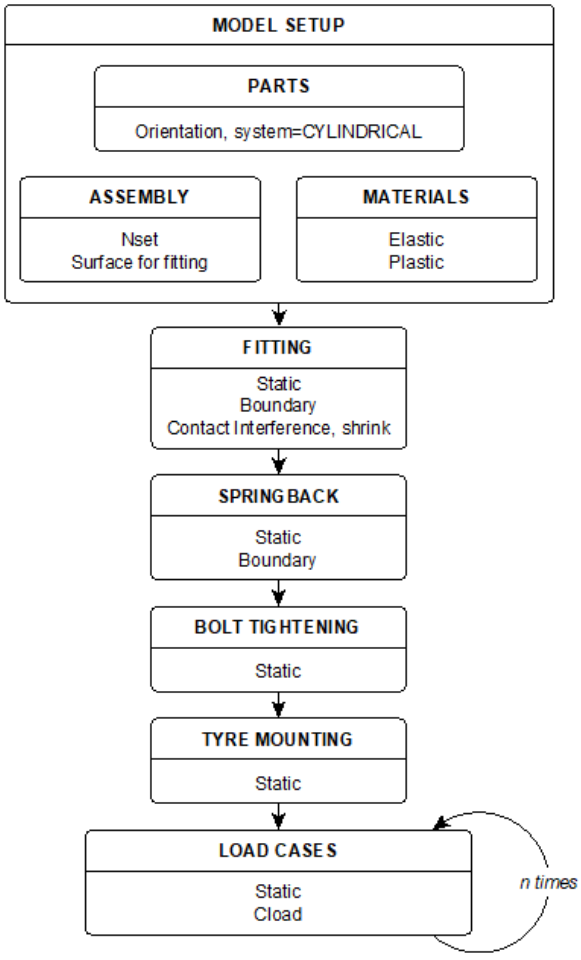

Figure 19. ABAQUS® input file structure.

3.2.5 Tire Inflation and Loading Steps

This paragraph focuses on how different loads are applied in the FE model. Due to the significant deformations that occur in the rubber tire, a nonlinear geometry analysis must be conducted to accurately capture the behaviour of the tire under loading.

First, the tire needs to be inflated to replicate the real-world conditions in which the tire is under internal pressure. This step is crucial for accurately simulating the tire's behavior, as inflation affects both the tire's shape and the forces it experiences. To ensure that the simulation runs smoothly and avoids convergence problems, two key steps are typically taken:

- *Initial Geometric Adjustment*: Before applying any pressure, the tire may need to undergo a preliminary deformation phase to account for its natural shape when not under pressure. This helps to create a realistic starting point for the analysis and reduces the chances of unrealistic initial behaviour.

- *Gradual Pressure Application*: The internal pressure is applied gradually in increments rather than all at once. This step-by-step approach allows the model to adapt to the deformation as the pressure increases, minimizing large, sudden changes that could cause the simulation to fail or converge incorrectly.

By performing these two steps, the model can avoid instability and ensure a smooth and accurate representation of the tire's deformation during inflation, which is critical for subsequent analysis of tire-rim interaction and overall performance.

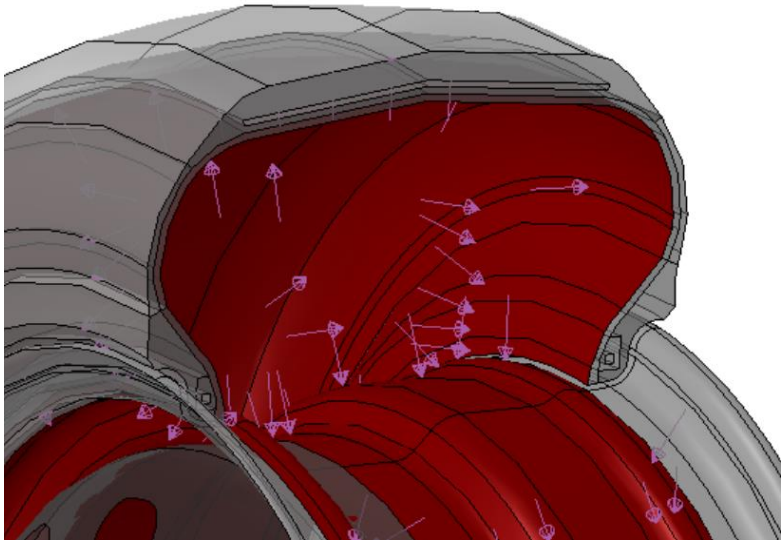

Figure 20. Inflating pressure application.

Once the tire is fully inflated, vertical and lateral loads (table 8) are applied in separate steps to simulate real-world operating conditions. To ensure that the applied forces precisely match experimental test cases for accurate comparison, the Force Control method is used. In this approach, forces are directly applied at the reference point (RP), which is coupled with the rigid surface of the disc hub. As a result, the deformation of the wheel occurs naturally based on its stiffness and structural response. This method allows for a realistic simulation of load distribution and ensures that the model behaves consistently with actual experimental conditions. To simulate different loading conditions:

- *For radial load analysis*, only one step is required, as this evaluates the tire's response to vertical force alone.

- *For biaxial load application*, two steps are necessary to properly introduce in a sequence vertical and lateral forces, ensuring accurate representation of the combined loading effects.

This stepwise approach helps maintain numerical stability and ensures that the simulation captures the realistic interaction between the tire and rim under different force conditions.

Table 8. Simulated load cases.

Load case	F_z [N]	F_y [N]	γ [°]
1	16104	-5086	14.4
2	4238	-1695	6.7
3	10171	-1695	5.2
4	5792	-1413	5.2
5	16104	0	0.0
6	7628	0	0.0
7	6357	283	0.0
8	10171	1695	-5.3
9	6498	1695	-7.6
10	7063	2825	-10.2
11	8970	4238	-13.6
12	12361	4309	-12.6
13	16104	5086	-14.4
14	10171	5227	-14.3
15	8829	5651	-14.3
16	10736	7063	-15.0
17	15257	7134	-15.0
18	13279	7134	-15.0
19	12714	8476	-15.0
20	14126	8970	-15.0
21	16881	9041	-15.0
22	20623	10311	-13.0

Chapter 4: Results and Discussion

4.1 Validation of assigned material properties

To ensure the accuracy and reliability of the material properties assigned within the finite element (FE) model, a validation process was conducted by calculating and comparing the radial stiffness of the wheel in both the numerical simulation and the physical experiment. The aim of this comparison was to determine whether the simulated mechanical behavior of the tire-wheel system corresponds closely with real-world performance under similar loading conditions.

The validation focuses on comparing results from two sources:

- The FEM simulation, developed in ABAQUS
- The experimental test campaign, in which an actual tire-wheel assembly was subjected to controlled loads in a laboratory environment.

The procedure is based on a relatively simple concept. In both the simulation and the physical test, a radial force is applied to a rigid steel plate positioned against the tire tread. As the load increases, the displacement of the plate, caused by the deformation of the tire, is recorded. This allows for the construction of a force-displacement curve, where the vertical axis (y-axis) represents the applied radial force and the horizontal axis (x-axis) represents the corresponding radial displacement of the plate.
In the experimental setup, the applied forces are measured using a 6-axis load cell placed directly beneath the steel contact plate. This setup allows for accurate real-time acquisition of the force transmitted through the tire. In the FEM model, the corresponding reaction force is not measured directly at the contact interface but is instead obtained from a designated reference point (RP1)—the only constrained node in the model, which acts as the mechanical interface between the tire and the hub of the disc. This point registers the reaction forces resulting from the deformation of the tire during the simulated loading process.
By comparing the slopes of the resulting force-displacement curves (i.e., the radial stiffness), it becomes possible to assess whether the mechanical response of the FEM model is consistent with the real-world behavior of the tire. A good correlation between the two indicates that the material properties defined in the simulation particularly those of the rubber compounds and reinforcements are appropriately chosen and capable of accurately reproducing the tire's structural response under radial loading.

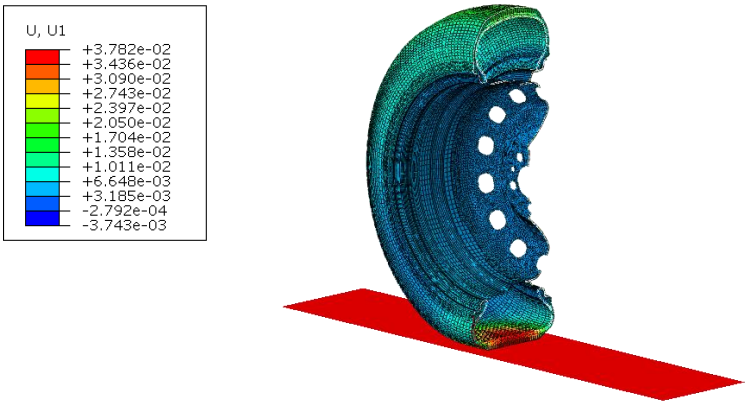

Figure 21. Radial displacement of the tire-plate contact point

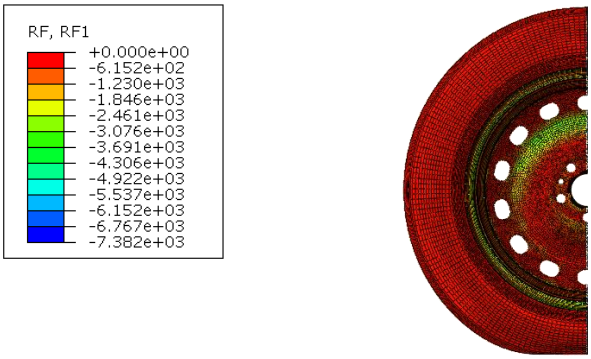

Figure 22. Vertical reaction force

The points on the curves in this way obtained, which are in all cases linear, are interpolated and the angular coefficient represents the radial stiffness of the wheel.

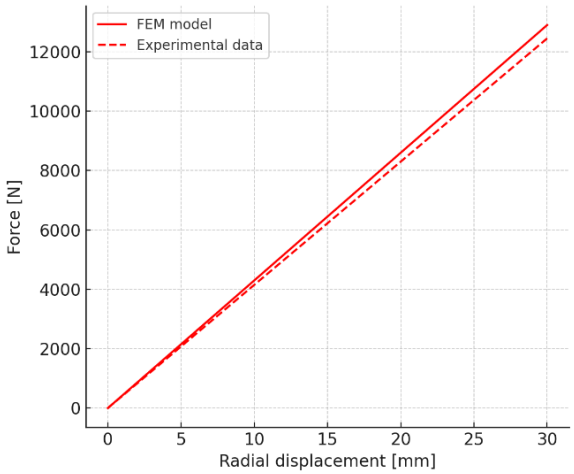

Figure 23. Comparison of FEM and Experimental Force–Displacement Response in Radial Direction.

Table 9. Comparison of Stiffnesses.

	Stiff. of FEM model [N/mm]	Stiff. of Experimental model [N/mm]	Error [%]
Inflation 5 bar	459.85	443.93	3.6

The comparison between the simulation results and experimental data reveals that the error in both simulated cases remains well below the 10% threshold. This relatively low level of deviation is considered acceptable, especially when one considers the inherent complexities involved in modeling a tire-rim system and the necessary simplifications introduced in the finite element model. These simplifications include geometric idealizations, assumptions about contact interactions, and the use of generalized material properties where exact data may be difficult to obtain.

Despite these approximations, the model demonstrates a high degree of consistency with experimental measurements, indicating that the core mechanical behavior of the tire has been effectively captured. One critical observation made during the analysis is that the rubber materials, which constitute a significant portion of the tire, play a particularly important role in influencing the overall stiffness. Their nonlinear, hyperelastic behavior must be accurately represented for the model to yield meaningful results. In this study, material parameters were derived from established data sources and calibrated for the intended application, resulting in good alignment with physical test results.

Furthermore, the validity of the simulated stiffness values is reinforced by previous research findings reported in literature sources [16, 21, 22], which support the use of similar modeling strategies and material definitions. Taking all of this into account the low error margins, the robustness of the model under realistic loading conditions, and the backing from existing academic work can be concluded with confidence that the material properties assigned in the FE model are reliable for the purpose of analyzing tire-rim interactions. This validation step strengthens the credibility of the model and confirms its suitability for further simulations and design assessments.

4.2 Contact Pressure

The first analysis is conducted on the FE model to examine the contact pressure at the rim flange after the "Clamped disk" step. At this stage, the tire remains uninflated. A subsequent analysis is performed after the "Tyre mount" step, where the tire is still not in contact with the drum surface. As a result, the forces F_t' and T_t' are null, and the pressure distribution remains uniform along the angular direction. This allows for the separation of the radial bead tension contribution $F_{b,r}$ from the opposing indirect radial effect caused by the hydrostatic force field F_p.

Figure 24 illustrates this effect, showing the contact pressure distribution for both the outer flange (left) and the inner flange (right). The blue lines represent the pressure distribution due solely to the bead-seat interference fit, while the red dashed lines depict the combined effect of inflation pressure and interference. This comparison highlights the influence of inflation pressure on the overall contact pressure distribution, providing insight into the load transmission at the tire-rim interface. The contact pressure is bidimensional value. The real values are highly

sensitive to the initial condition and real dimensions of the tire that is experimental tests. However, the contact pressure trend is highly correlated with experimental value.

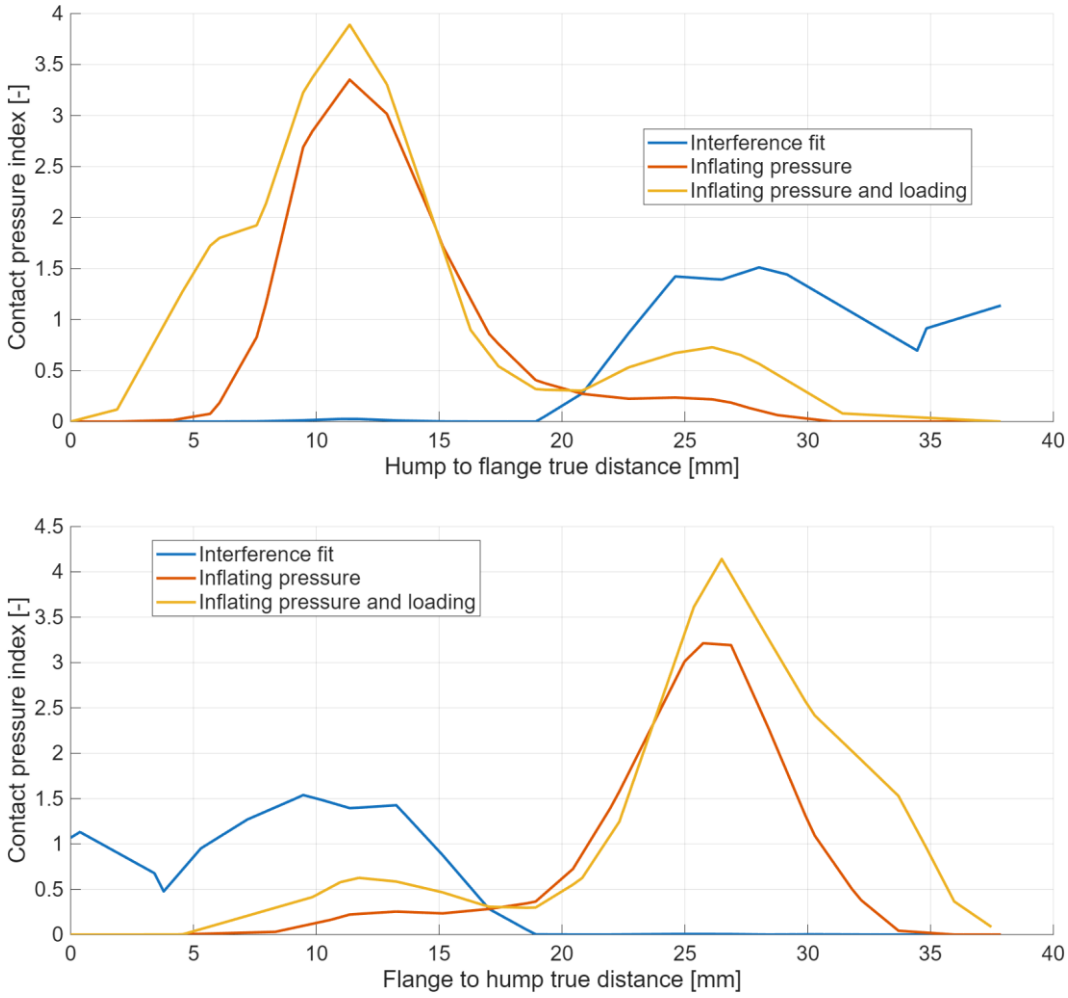

Figure 24. Simulation results of contact pressure distribution by the loading case #5

In the step "Clamped disk" the interference fit primarily affects the hump regions, specifically in the 20mm to 40mm and 0mm to 20mm of true distance between flange and hump. Here, the pressure is concentrated in a small section, creating a peak at the minimum bead distance position. This peak is influenced by the fact that the outer flange is closer to the rim-disc interference region, which acts as a cantilever constraint. Conversely, the flange regions, corresponding to the 0mm to 20mm and 20mm to 40mm of true distance, experience minimal loading. The contact pressure in these areas is mainly due to the elastic bending of the sidewall, and their response remains nearly identical, as it is primarily dependent on hydrostatic behaviour. Additionally, an intermediate unloaded region exists due to the different curvatures of the rim flange and sidewall, preventing contact.

Following the inflation step, the flange regions become significantly loaded by the hydrostatic force field. The behaviour of the hump regions is particularly noteworthy: although the hydrostatic force does not directly act on the hump, the overall pressure increase causes the tire to expand radially. This radial expansion

places the bead under tension, consequently reducing the radial force contribution, $F_{b,r}$.

The developed FE model aligns with the experimental pressure fields reported in [50], while also highlighting the minimal variation in the magnitudes of radial forces acting on the rim flanges. The loading conditions are analysed by inducing the ABAQUS® simulated load through kinematically imposed tire deformation. This method allows for the replication of side-wall deformation, which in turn generates the corresponding reaction forces. Figures 25 and 26 present a comparison between the deformations obtained using the software and the proposed approach. On the left side of each figure, the graphical output at steady-state conditions is displayed, while the middle section shows the deformation state imposed on the nonlinear 3D FE model with a stiff interface. On the far right, the von Mises stress map confirms the proper transmission of loads to the wheel structure.

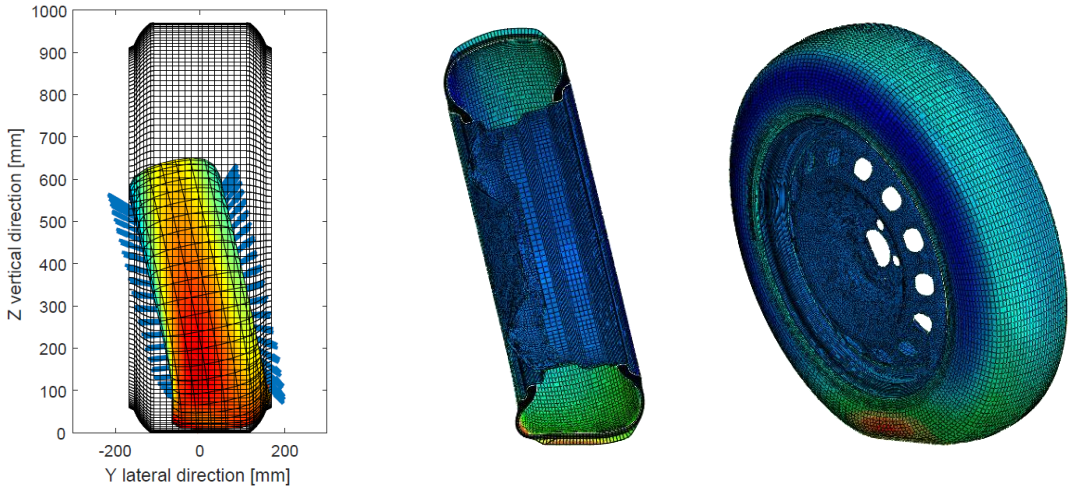

Figure 25. 0215X wheel under ZWARP load case #1 (γ = 14.4°): ABAQUS results (left) and stiff distributed interface imposed kinematics (right).

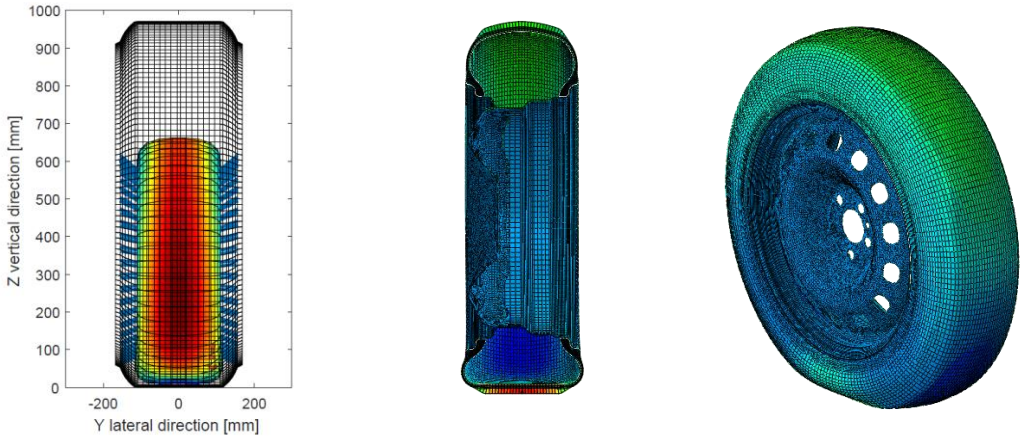

Figure 26. 0215X wheel under ZWARP load case #6 (γ = 0°): ABAQUS results (left) and stiff distributed interface imposed kinematics (right).

4.3 Comparison of numerical and experimental data

Finally, the experimental strain measurements are compared with numerical results obtained using the rigid interface developed in this FE model. Numerical data is extracted based on the strain gauge positions from Table 5.5. Unlike the experimental tests, where absolute wheel orientation may vary, the ABAQUS® results provide a fixed reference. By using the initial tire orientation, which remains consistent throughout the pre-simulation, a single wheel revolution is isolated from the computed results in ABAQUS®. In this revolution, the 0° angular position corresponds to the centre of the contact patch against the drum. In Figure 27 it is shown the analysis results, the Von Mises stress of each load cases, an index of the proper loading condition occurring.

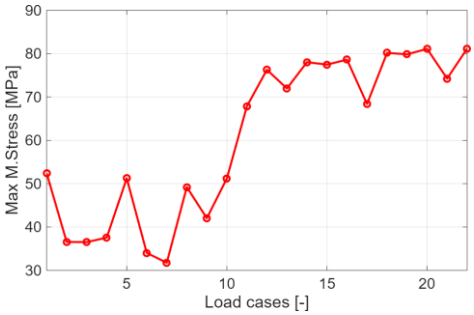

(a) R1 radial outer hump.

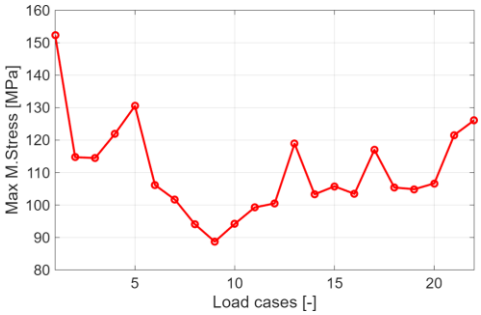

(d) R4 radial inner hump.

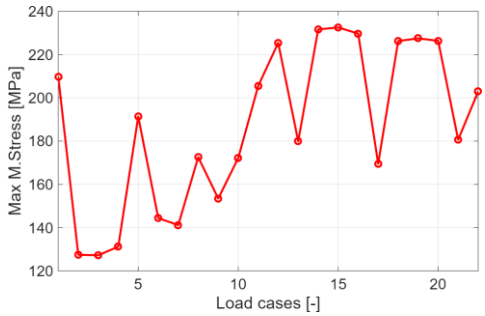

(b) R2 crf. outer hump.

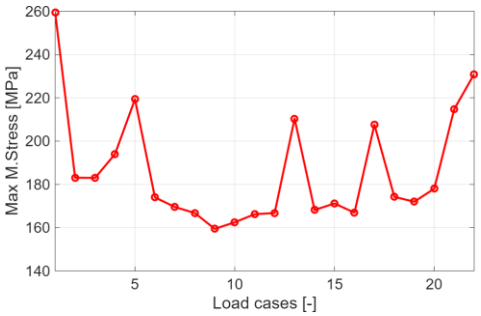

(e) R5 crf. inner hump.

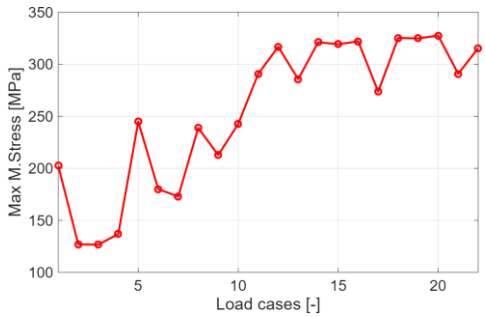

(c) R3 crf. outer flange.

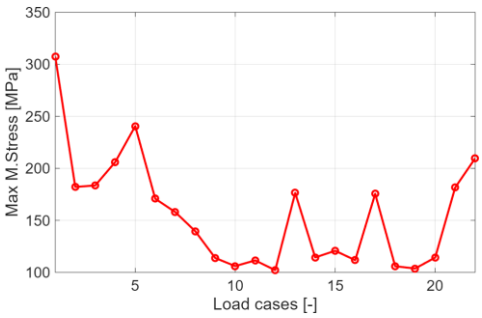

(f) R6 crf. inner flange.

Figure 27. Max V. Mises stresses related to flange experimental strain gauge measurements.

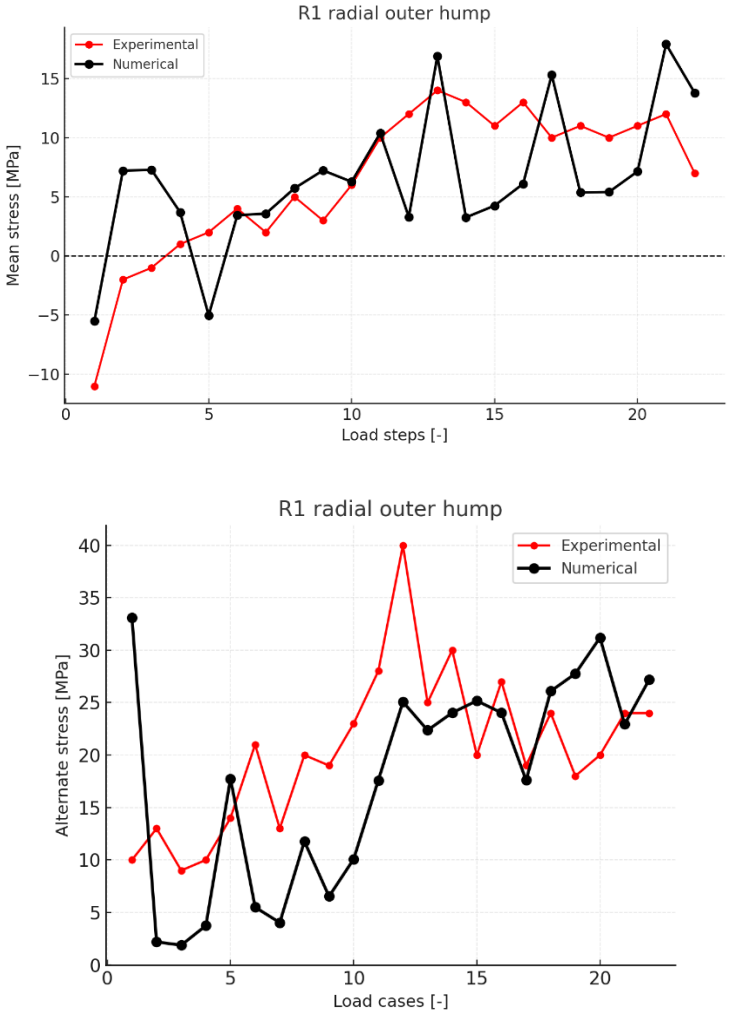

Figure 28. Comparison between experimental and numerical results of mean and alternate stresses of R1 radial outer hump.

Figure 28 shows the comparison between experimental and numerical results at the R1 strain gauge location on the radial outer hump demonstrates good agreement in both mean and alternate stress trends across the 22 load cases. The mean stress plot shows that the numerical model closely follows the experimental data, particularly under higher loading conditions, with minor deviations observed at lower load steps. The alternate stress comparison highlights a tendency of the numerical model to overestimate stress amplitudes in early load cases, likely due to an overestimation of sidewall stiffness in the simplified tire model. Despite these discrepancies, the model effectively captures the overall stress evolution, confirming its reliability for fatigue assessment in the rim flange region.

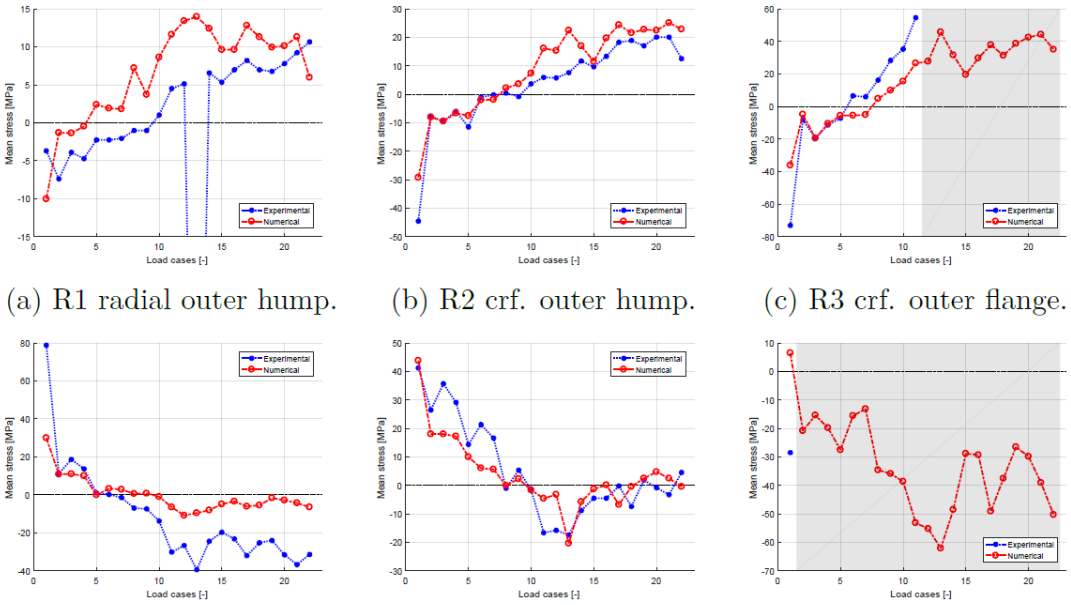

(a) R1 radial outer hump. (b) R2 crf. outer hump. (c) R3 crf. outer flange.

(d) R4 radial inner hump. (e) R5 crf. inner hump. (f) R6 crf. inner flange.

Figure 29. Mean stresses related to experimental strain gauge measurements.

Figure 29 illustrates the correlation between the mean stress values recorded at each strain gauge location, providing insight into the effectiveness of the loading conditions applied during testing. The results reveal a strong agreement in the circumferential direction on the hump region, indicating that the model accurately captures the dominant stress paths along this direction. However, under conditions involving high lateral loads, the radial stress component on the inner hump is consistently underestimated. This suggests a limitation in the numerical model's ability to replicate the true stiffness and deformation behaviour of the sidewall in that region. As lateral forces increase, the discrepancy becomes more pronounced, highlighting the sensitivity of radial stress predictions to sidewall dynamics and contact interface fidelity.

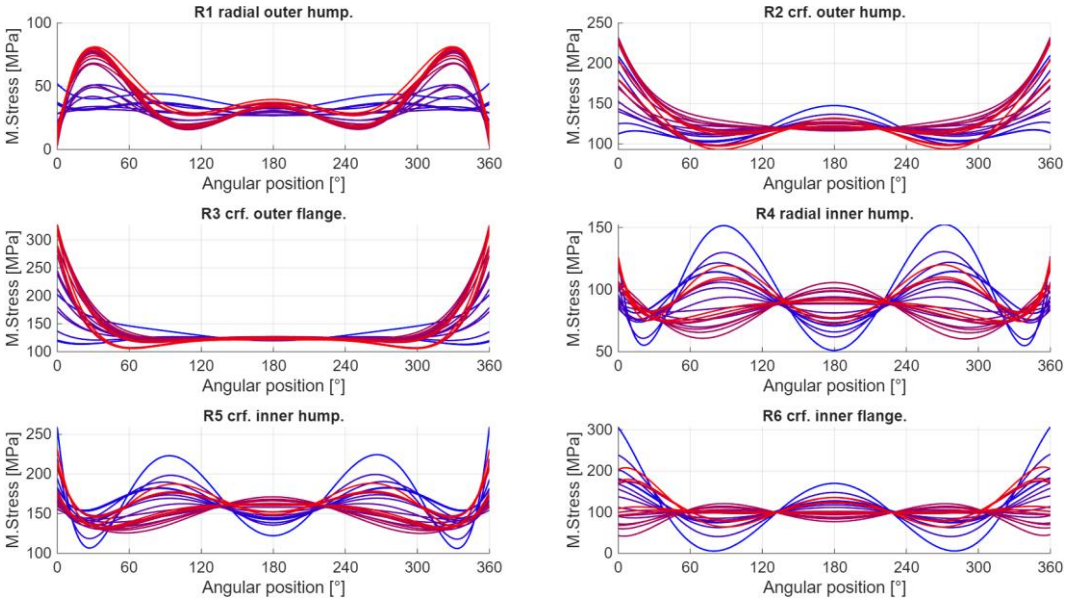

Figure 30. Angular V. Mises stress histories related to flange experimental strain gauge measurements.

Figure 30 shows experimental angular stress histories for all load cases. The six figures display corresponding stress data, where the colour gradient from blue to red represents increasing load case numbers—blue indicating load case #1 and red representing load case #22. The top row contains numerical results, while the bottom row shows experimental measurements. The plots show the Von Mises stress distribution along the angular position 0°–360° for each strain gauge (R1–R6), where 0° corresponds to the center of the contact patch. These results provide valuable insight into the stress behavior around the wheel circumference under various load cases (with blue lines indicating lower and red lines indicating higher load cases). 0° and 180° angular positions consistently coincide with stress peaks due to tire contact at the bottom and the force balance on the top. The outer flange and hump (R2, R3) are heavily loaded in both radial and circumferential directions, especially under high lateral and camber loads. The inner regions (R4, R5, R6) tend to unload under increasing side loads, reflecting a progressive shift in load path toward the outer rim areas.

Asymmetry in stress distributions, especially in R3 and R6, suggests increasing lateral bias and possibly uneven tire deformation due to camber and lateral force application.

The discussion focuses on strain gauges R1 to R6, as they are more relevant to the study's objectives. A more comprehensive analysis, including all strain gauge comparisons, is available in Appendix.

Chapter 5: Conclusion and Future work

5.1 Conclusion

This thesis has presented a comprehensive investigation into the nonlinear interaction between automotive tire sidewalls and steel wheel flanges using advanced finite element (FE) modeling techniques validated against rigorous experimental data.
A detailed FE model was developed in ABAQUS, capturing the essential nonlinearities, material behaviors, and contact phenomena at the tire-rim interface. The rim was modeled using shell elements to balance accuracy and computational efficiency, while the tire was represented with layered hexahedral elements employing hyperelastic material models. Critical aspects such as bead-seat interference, inflation pressure, and complex contact conditions (including both frictional and frictionless regions) were explicitly incorporated.
Experimental validation was conducted using a robust strain gauge setup, strategically positioned based on a strain-geometrical selection criterion. Strain measurements collected under a matrix of biaxial loading conditions provided high-quality data for comparison with simulation results.

Key outcomes include:

- The FE model reliably predicted contact pressures, stress distributions, and strain histories at critical locations, demonstrating high correlation with experimental data.
- The model accurately captured the redistribution of contact pressures resulting from inflation and loading and effectively identified regions susceptible to fatigue or failure.
- Discrepancies observed between simulation and experiment were limited and generally attributable to practical constraints (e.g., material property variability, simplified friction modeling, and manufacturing tolerances).

The methodology established in this thesis provides a validated framework for simulating tire-rim interactions, enabling engineers to optimize wheel designs for weight, durability, and performance while reducing reliance on physical prototyping.

5.2 Limitations

While the research achieved its main objectives, certain limitations are acknowledged:

- *Material Assumptions:* The use of homogeneous and literature-based properties for rubber compounds does not fully capture potential local variations, anisotropy, or aging effects present in real tires.
- *Friction Modeling:* Friction coefficients were based on published values; more precise measurements or dynamic friction modeling could further improve accuracy, especially under varying operating conditions.
- *Computational Demands:* High-fidelity nonlinear FE analysis remains resource-intensive, which can restrict its routine application in early-phase design optimization or in contexts requiring rapid iteration.

5.3 Recommendations and Future Work

Building on the achievements and insights of this thesis, several opportunities for future research are recommended:

1. *Advanced Material Characterization:*
   Perform detailed experimental characterization of tire materials, including rate-dependent (viscoelastic) and anisotropic properties, to enhance the fidelity of FE models.
2. *Dynamic and Transient Loading:*
   Extend the FE modeling framework to include dynamic and transient loading scenarios (e.g., sudden braking, cornering maneuvers, or impact loads), to better reflect real-world operational environments.
3. *Fatigue and Failure Prediction:*
   Integrate fatigue life prediction methods and crack initiation models into the FE simulation to more directly assess wheel durability over a vehicle's lifecycle.
4. *Parametric and Sensitivity Studies:*
   Conduct comprehensive parametric studies on geometric (e.g., flange thickness, bead profile) and material parameters, as well as friction coefficients, to quantify their influence on stress distribution and wheel performance.
5. *Optimization and Surrogate Modeling:*
   Leverage the validated FE model to support design optimization, possibly incorporating surrogate modeling or reduced-order models—to enable faster design iteration and automated optimization routines.
6. *Industrial Application and Customization:*
   Collaborate with industry partners to apply and further refine the model on a wider variety of wheel and tire types, accounting for specific design and manufacturing constraints.

5.4 Final Remarks

The research presented in this thesis advances the understanding and simulation of tire-rim interactions, providing a solid foundation for improved virtual design, durability assessment, and lightweighting of automotive wheels. The developed methodology, validated by targeted experiments, positions FE modeling as a reliable tool for future wheel engineering challenges and offers a pathway toward reduced development cycles and enhanced product performance.

Appendix

Experimental-numerical comparison of strain gauge analysis

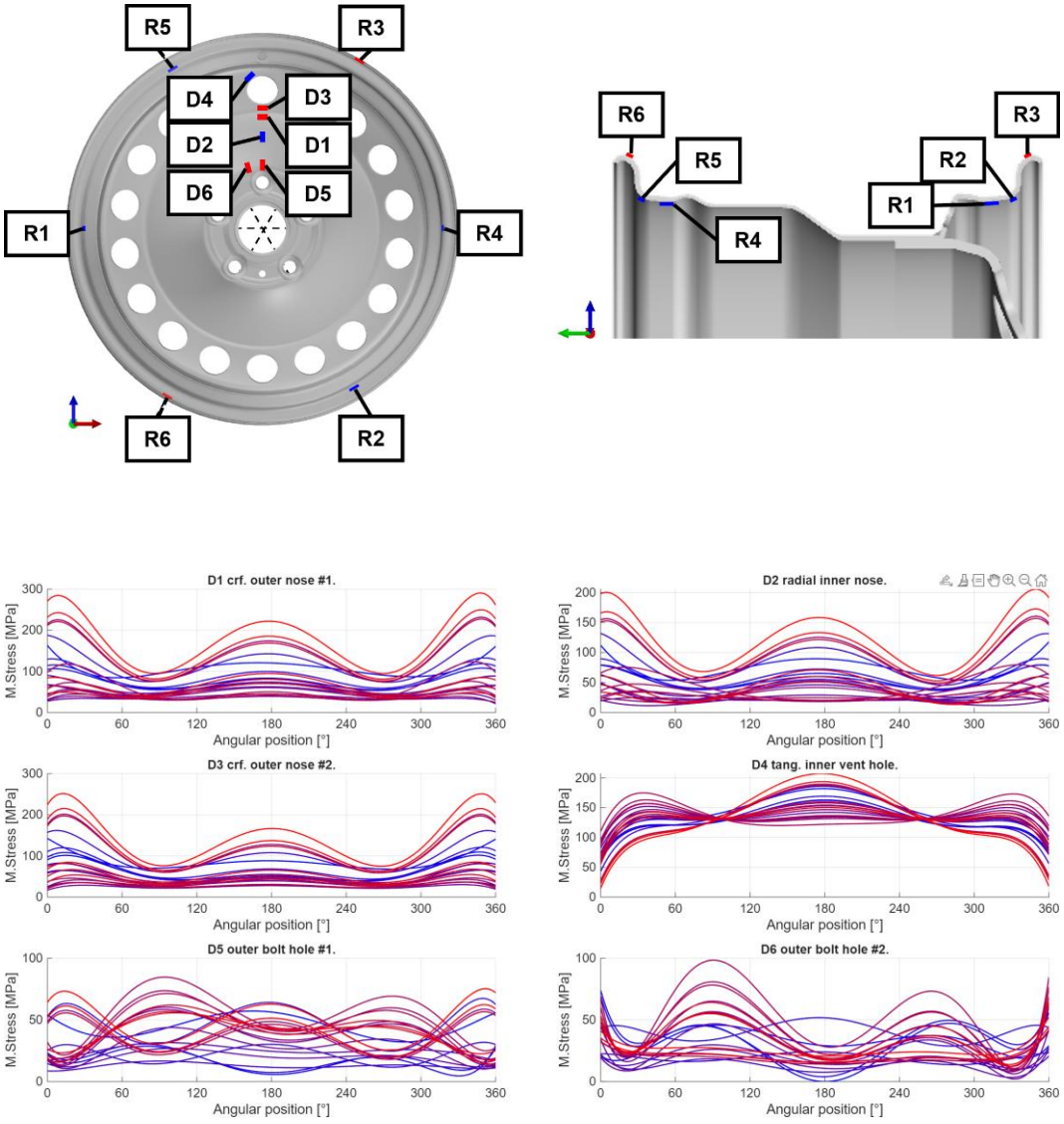

Figure 31. Angular V. Mises stress histories related to disc experimental strain gauge measurements.

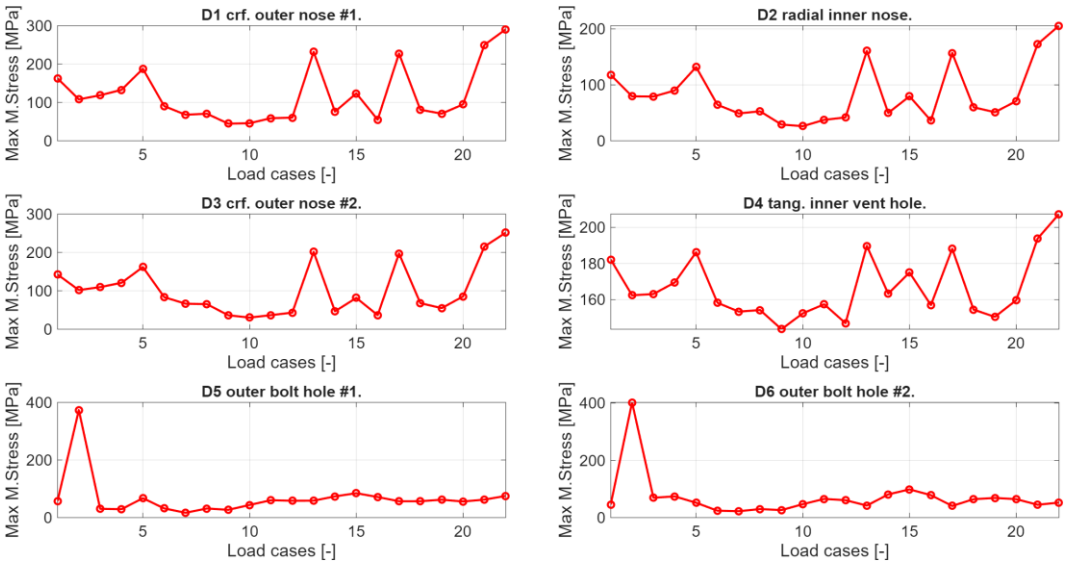

Figure 32. Max V. Mises stresses related to disc experimental strain gauge measurements.

Reference

[1] ETRTO—European Tyre and Rim Technical Organisation, Standards manual 2020, 2020.

[2] Association of European Wheel Manufacturers, EUWA ES-3 wheel technical specification standard, 2017.

[3] ISO 3894:2015 road vehicles — wheels/rims for commercial vehicles — test methods.

[4] SAE J328 wheels — passenger car and light truck performance requirements and test procedures, 2021.

[5] SAE J2562 biaxial wheel fatigue test, 2021.

[6] M. Firat et al., “Numerical modeling and simulation of wheel radial fatigue tests”, 2009.

[7] U. Kocabicak and M. Firat, “Numerical analysis of wheel cornering fatigue tests”, 2001.

[8] P. R. M. Raju et al., “Evaluation of fatigue life of aluminum alloy wheels under radial loads”, 2007.

[9] F. M. Santiciolli et al., “Simulation of the scenario of the biaxial wheel fatigue test”, 2017.

[10] D. Shang et al., “Research on the stamping residual stress of steel wheel disc and its effect on the fatigue life of wheel”, 2016.

[11] J. C. Stearns et al., “Modeling the mechanical response of an aluminum alloy automotive rim”, 2004.

[12] X. Wan et al., “Simulation of biaxial wheel test and fatigue life estimation considering the influence of tire and wheel camber”, 2016.

[13] Z.-G. Zheng et al., “Numerical simulation of steel wheel dynamic cornering fatigue test”, 2014.

[14] M. Lamé, Leçons sur la théorie mathématique de l’élasticité des corps solides. 1866.

[15] E. Bonisoli, C. Delprete, and C. Rosso, “Modal-geometrical-based master nodes selection criterion in modal analysis”, 2009.

[16] T. D. Gillespie, Fundamentals of Vehicle Dynamics. SAE International, 1992.

[17] M. Guiggiani, The Science of Vehicle Dynamics. Springer, 2018.

[18] K. Cosseron et al., “Optimized gauging for tire–rim loading identification”, 2021.

[19] K. Cosseron et al., “Optimal parameterization of tire–rim interaction for aircraft wheels”, 2019.

[20] J. C. Stearns et al., “Analysis of stress and strain distribution in a vehicle wheel: Finite element analysis versus the experimental method”, 2005.

[21] H. Pacejka and I. J. Besselink, Tire and Vehicle Dynamics. Elsevier, 2012.

[22] F. Ballo et al., “A semi-analytical tyre model for the study of tyre/rim interaction on a road vehicle”, 2017.

[23] F. Ballo et al., “Tire-rim interaction, a semi-analytical tire model”, 2018.

[24] M. Gipser, “ADAMS/FTire-a tire model for ride & durability simulations”, 2000.

[25] M. Gipser, “FTire – the tire simulation model for all applications related to vehicle dynamics”, 2007.

[26] I. Besselink et al., “The SWIFT tyre model : Overview and applications”, 2004.

[27] A. Gallrein and M. Bäcker, “Cdtire: A tire model for comfort and durability applications”, 2007.

[28] cosin scientific software AG. “FTire/rim - extension to ftire/core for flexible and visco-plastic rim modelling”, 2022.

[29] D. Socie and G. Marquis, Multiaxial fatigue. SAE International, 1999.

[30] E. Bonisoli et al., “Improvements on design and validation of automotive steel wheels”, 2019.

[31] J. E. Shigley, Standard Handbook of Machine Design. McGraw-Hill, 2004.

[32] S. Bhattacharyya et al., “Failure analysis of cracking in wheel rims – material and manufacturing aspects”, 2008.

[33] J. A. Sherwood et al., “An investigation of tire-wheel interface loads using ADINA”, 1995.

[34] J. A. Sherwood et al., “Study of the pressure distribution on an aircraft tire–wheel interface”, 1995.

[35] J. D. Walter and R. Kiminecz, “Bead contact pressure measurements at the tire-rim interface”, 1975.

[36] S. Kandarpa et al., “Determination of tire-wheel interface loads for aircraft wheels”, 1994.

[37] D. J. Kirkner et al., “Determination of tire-wheel interface pressure distribution for aircraft wheels”, 1993.

[38] E. Schudt et al., “Three-dimensional verification of an axisymmetric algorithm for tire-wheel interface load recovery”, 1994.

[39] B. F. Spencer Jr. et al., “Experimental verification of an algorithm for determination of tire-wheel interface loads”, 1995.

[40] X. Wan et al., “Tire-rim interface pressure of a commercial vehicle wheel under radial loads: Theory and experiment”, 2017.

[41] Tekscan, Inc. “Pressure mapping sensor 8110”, 2015.

[42] H. Guo et al., “Development of a detailed aircraft tyre finite element model for safety assessment”, 2014.

[43] W. Hall et al., “Tire modeling methodology with the explicit finite element code ls-dyna”, 2004.

[44] N. D. Korunović et al., “Fea of tyres subjected to static loading”, 2007.

[45] N. D. Korunović et al., “Finite element analysis of a tire steady rolling on the drum and comparison with experiment”, 2011.

[46] Fujifilm. “Prescale pressure measurement film”, 2021.

[47] S. K. Clark, Mechanics of pneumatic tires. US Government Printing Office, 1971.

[48] G. A. Holzapfel, Nonlinear Solid Mechanics: A Continuum Approach for Engineering. Wiley, 2000.

[49] E. Bonisoli et al., “Hardware and virtual test-rigs for automotive steel wheels design”, 2020.

[50] J. D. Walter and R. Kiminecz, “Bead contact pressure measurements at the tire-rim interface”, in *1975 Automotive Engineering Congress and Exposition, Detroit, MI, 24 February 1975, SAE International, Feb. 1975. doi: 10.4271/750458.*